TECHNISCHE UNIVERSITÄT WIEN
Vienna | Austria

202.057 Mechanical properties of biological tissue

Micro- and macro-mechanical tests

Microscopy techniques

Luis ZELAYA-LAINEZ

Contact information

- Dipl.-Ing. Dr.techn. **Luis ZELAYA-LAINEZ**, MSc.
- Email: Luis.Zelaya@tuwien.ac.at

- Office:

Room AA 02 22

Karlsplatz 13

1040 Wien

Office hours need to be agreed beforehand!

If possible, due to the ongoing Coronavirus (COVID-19) pandemic, I prefer to be contact via email.

Nanoindentation

- Nanoindentation is widely recognized as the preferred method for testing thin film and surface mechanical properties.

Nanoindentation

- load, displacement, and contact area for any punch can be described as a solid of revolution of a smooth function
- Load-displacement relationship

$$P = \alpha h^m$$

- P is the indenter load
- h is the elastic displacement of the indenter
- α and m are constants
  - $m = 1$ for flat cylinders
  - $m = 2$ for cones
  - $m = 1.5$ for spheres in the limit of small displacements
  - $m = 1.5$ for paraboloids of revolution.

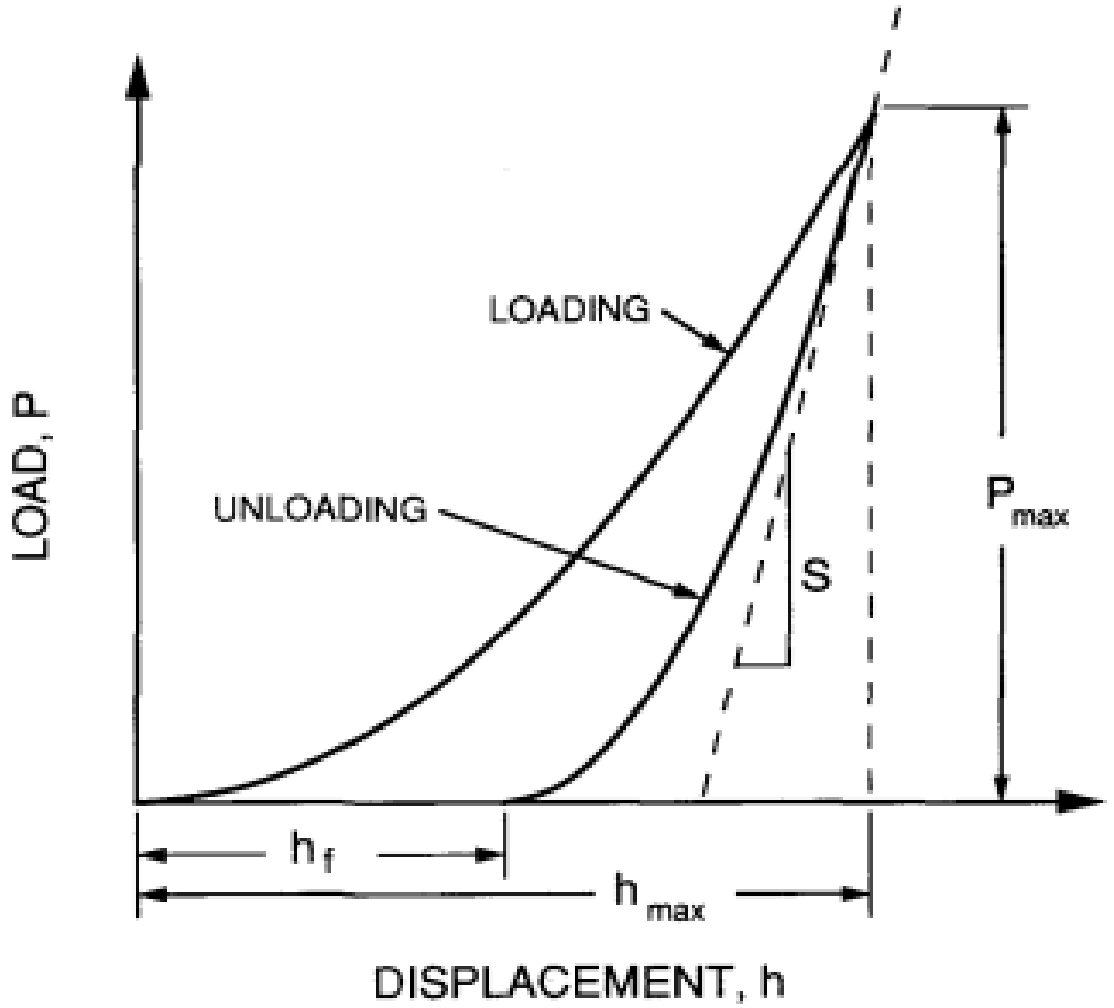

Nanoindentation

- Modeling indentation contact in a way that includes plasticity is a much more complex problem.
- Constitutive equations are nonlinear and a number of material parameters must be included to describe material behavior

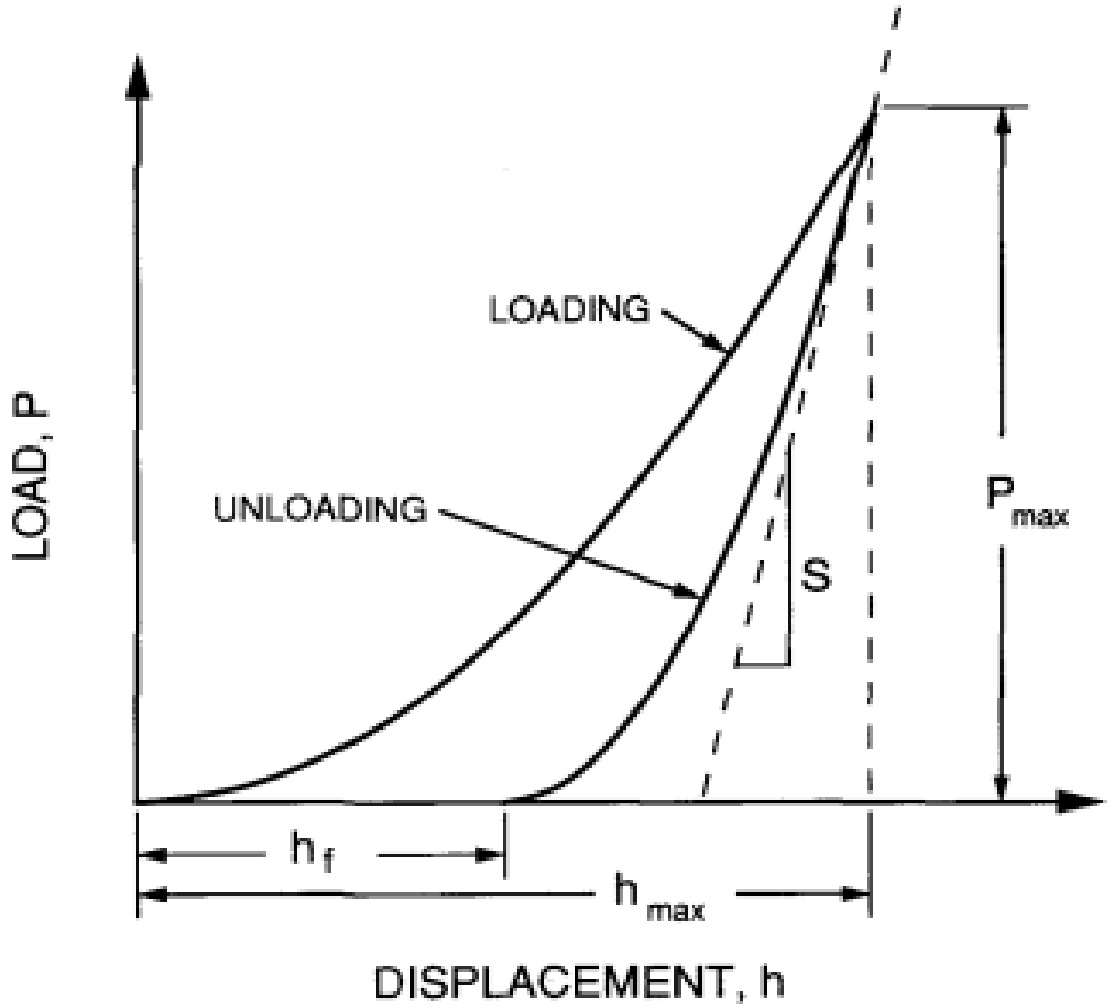

Nanoindentation

- Tabor and Stillwell were one of the first ones who experimented loading and unloading of conical tips. They discover the following:
  - the diameter of the contact impression in the surface formed by conical indenters does not recover during unloading—only the depth recovers
  - the indentation must be loaded and unloaded a few times before the load displacement behavior becomes perfectly reversible; i.e., a limited amount of plasticity sometimes occurs in each of the first few loadings and unloadings
  - effects of non-rigid indenters on the load-displacement behavior can be effectively accounted for by defining a reduced modulus, E_r

$$\frac{1}{E_r} = \frac{(1-\nu^2)}{E} + \frac{(1-\nu_i^2)}{E_i}$$

Tabor D (1948) A simple theory of static and dynamic hardness. *Proc. R. Soc. Lond*. A192 247–274

N A Stilwell and D Tabor (1961) Elastic Recovery of Conical Indentations. *Proc. Phys. Soc.* 78 169

Nanoindentation

$$\frac{1}{E_r} = \frac{(1-\nu^2)}{E} + \frac{(1-\nu_i^2)}{E_i}$$

- E is the Young's modulus of the specimen
- ν is th Poisson's ratio of the specimen
- E_i is the Young's modulus of the indenter
- ν_i is the Poisson's ratio of the indenter

- In the case of a diamond Berkovich tip, $E_i = 1140$ GPa and $\nu_i = 0.07$
- The Poisson's ratio of materials (specimens) oscillate between 0 and 0.5, typically they are 0.3.
- The Poisson's ratio is typically obtained by means of ultrasonic testing.

Nanoindentation

$$S = \frac{dP}{dh} = \frac{2}{\sqrt{\pi}} E_r \sqrt{A}$$

- $\frac{dP}{dh}$ is experimentally measured stiffness of the upper portion of the unloading data
- A is the projected area of the elastic contact.

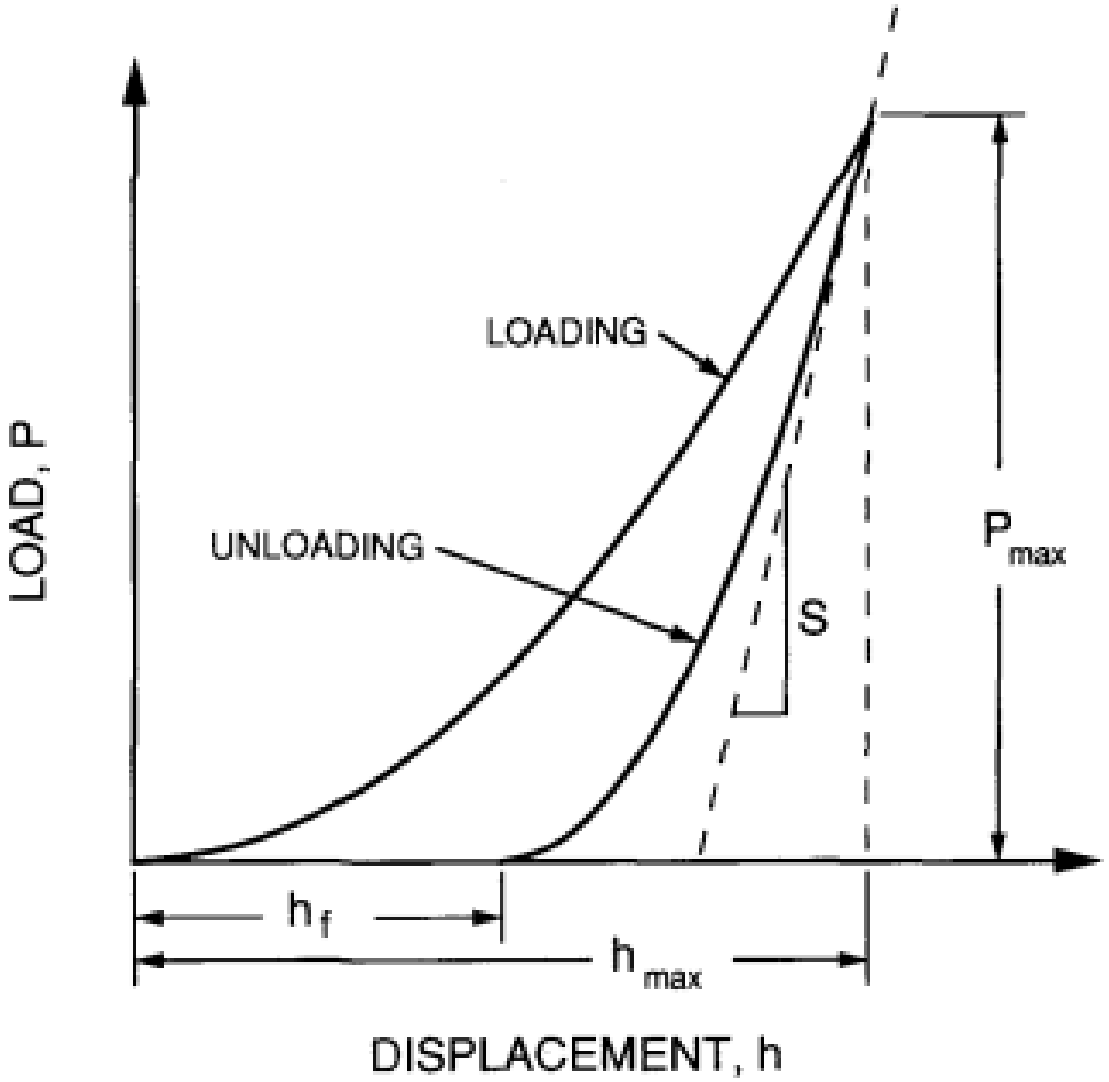

Nanoindentation

- By measuring the initial unloading stiffness and assuming that the contact area is equal to the optically measured area of the hardness impression, the modulus can thus be derived.
- However, a method based on measured indentation load-displacement curves and a knowledge of the indenter area function (or shape function), that is, the cross sectional area of the indenter as a function of the distance from its tip, can give the area of contact.

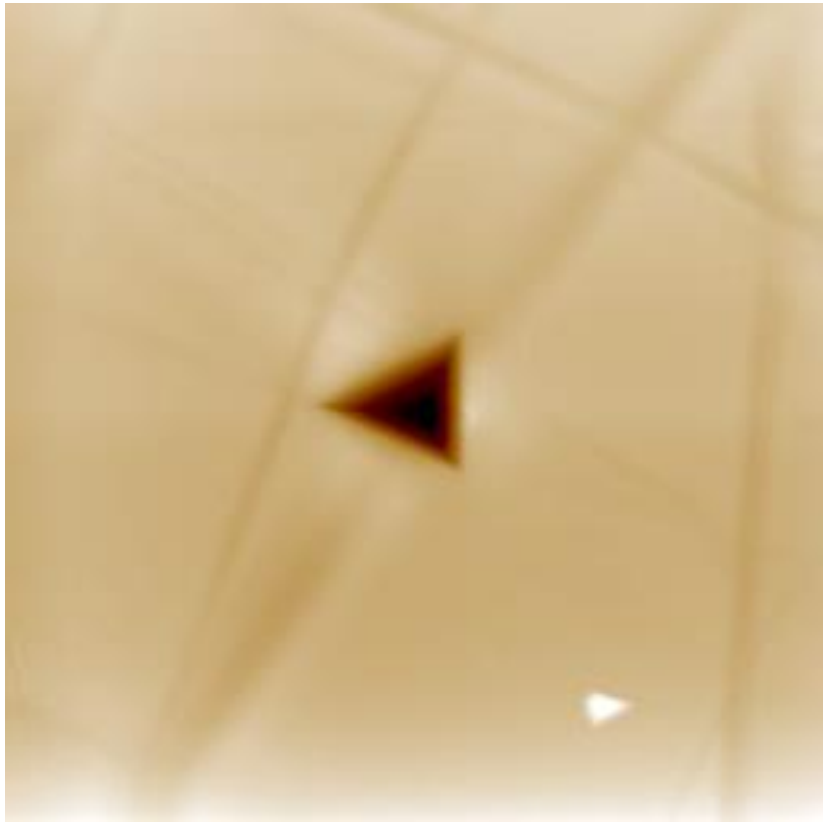

Nanoindentation

- Two obvious choices for the depth, though not the only ones, are the depth at peak load, h_{max} (i.e., the maximum displacement in the loading cycle), and the final depth, h_f (i.e., the residual depth of the hardness impression after final unloading), both of which are easily determined from indentation load-displacement data
- However, using TEM replication methods to establish the shape function, Oliver, Hutchings, and Pethica found that the final depth gives a better estimate of the contact area than the depth at peak load.

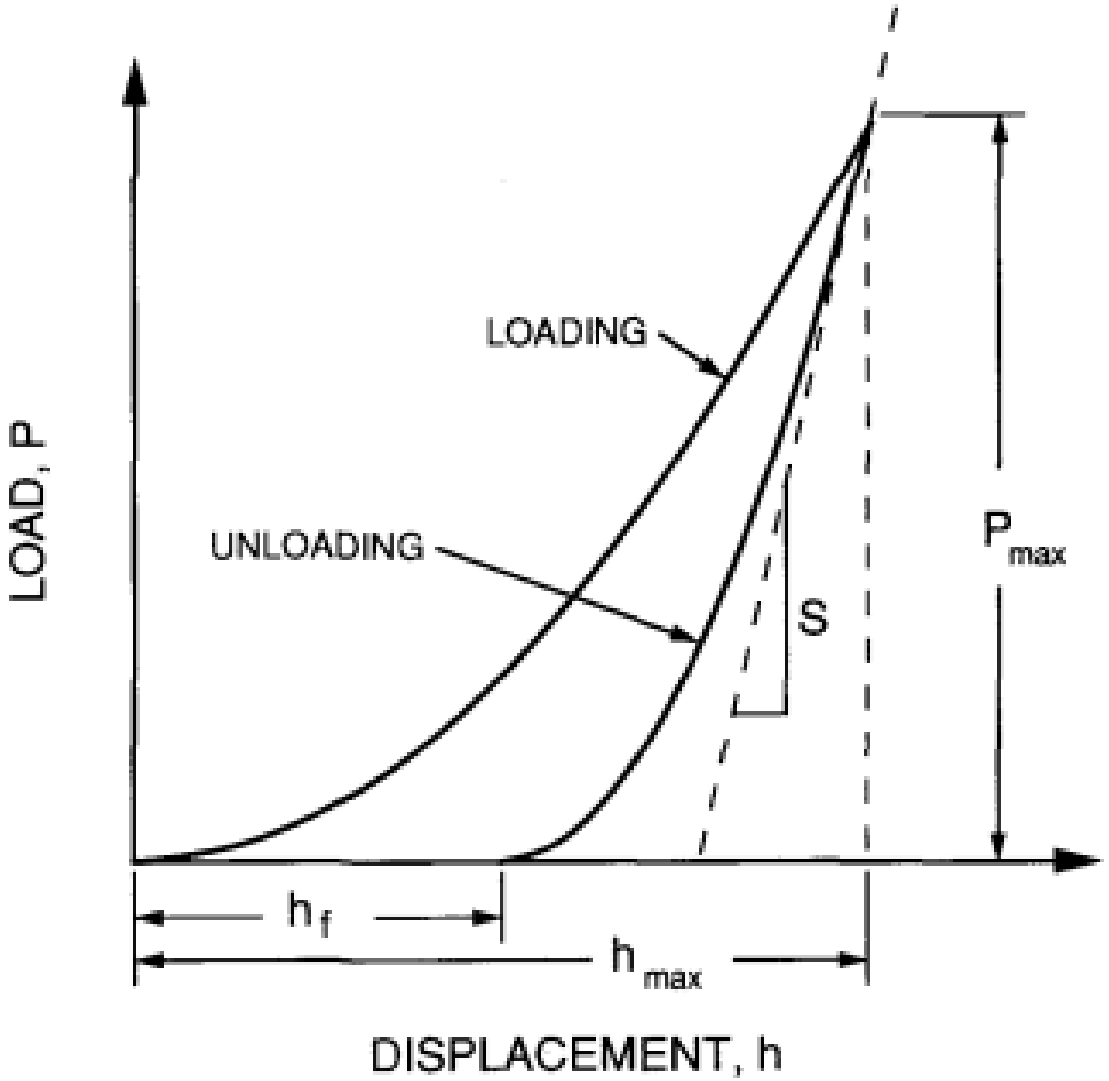

W. C. Oliver, R. Hutchings, and J. B. Pethica, in ASTM STP 889, edited by P. J. Blau and B. R. Lawn (American Society for Testing and Materials, Philadelphia, PA, 1986), pp. 90-108.

Oliver and Pharr method

- Paper published in 1992
- 26322 citations
- W. C. Oliver and G. M. Pharr (1992) An improved technique for determining hardness and elastic modulus using load and displacement sensing indentation experiments. *Journal of Materials Research*.

Warren Oliver

George M. Pharr

Oliver and Pharr method

- Since the revolutionary studies from Oliver and Pharr on the determination of elasticity and hardness of an elasto-plastic half-space by means of a 3-sided pyramid indenter, nanoindentation has become the predilect and a crucial technique to explore the material characterization at the micron and submicron scale.

- Normally, the 3-sided pyramid indenter is made of diamond and it is called a Berkovich tip.

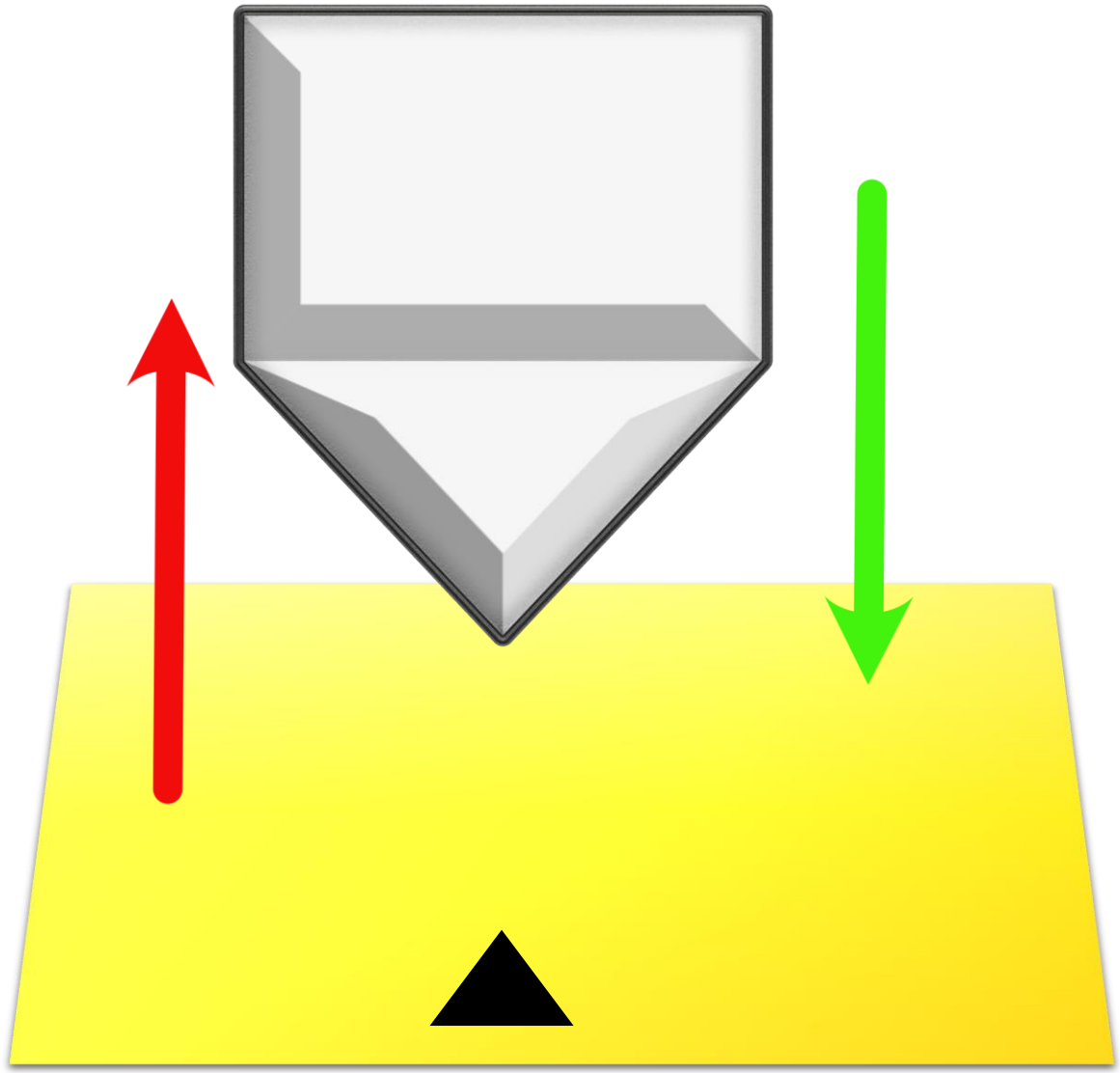

Oliver and Pharr method

- At any time during loading:

$$h = h_c + h_s$$

- h is the total displacement
- h_c is the vertical distance along which contact is made (called the contact depth)
- h_s is the displacement of the surface at the perimeter of the contact.
- a is radius of the contact

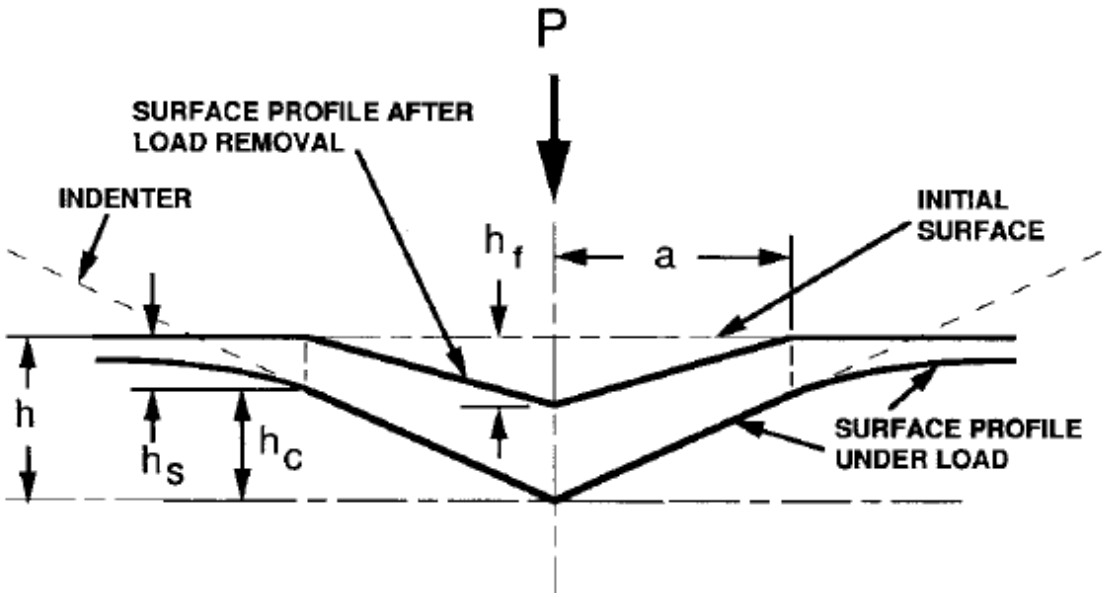

Oliver and Pharr method

- At peak load, the load and displacement are P_{max} and h_{max}
- Upon unloading, the elastic displacements are recovered, and when the indenter is fully withdrawn, the final depth of the residual hardness impression is h_f

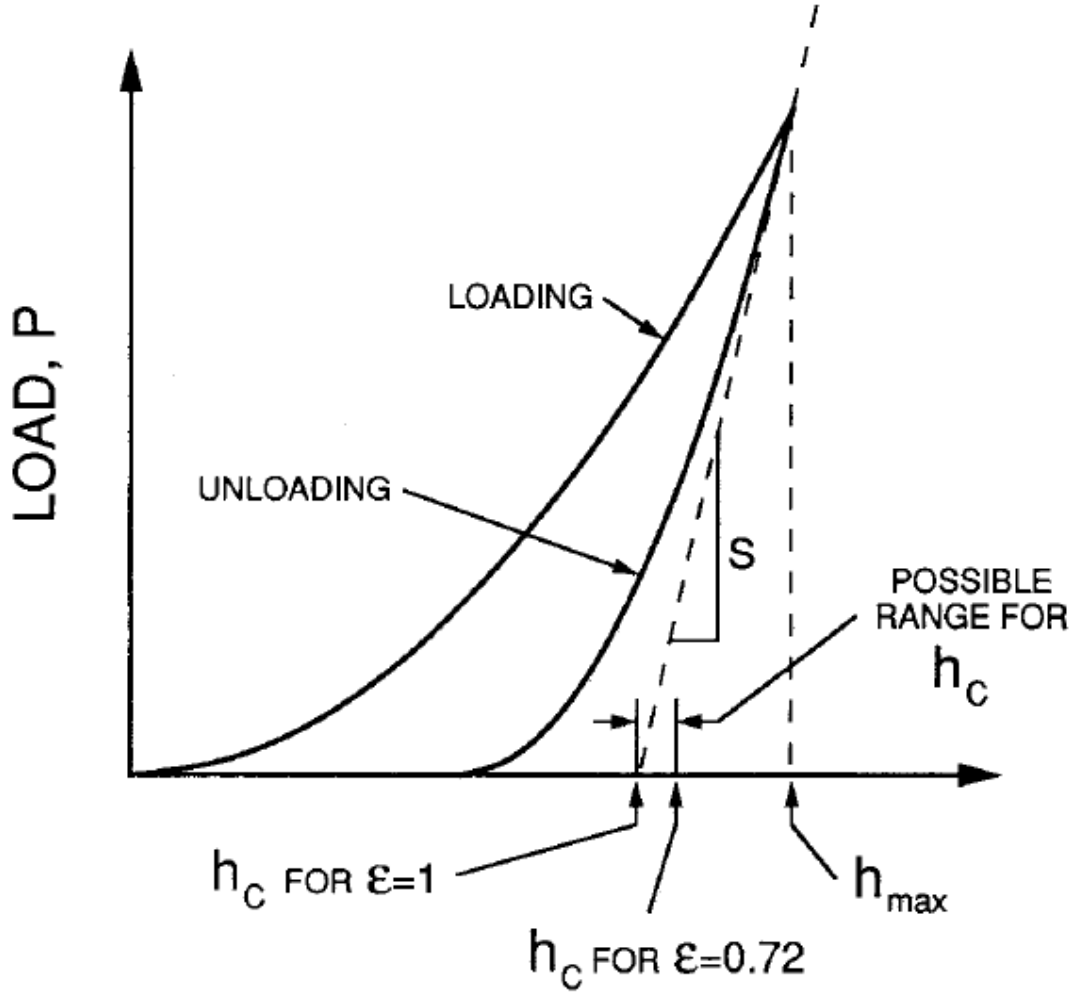

Oliver and Pharr method

$$E_r = \frac{\sqrt{\pi} S}{2\sqrt{A_c}}$$

- E_r is the reduced elastic modulus
- S is the measured stiffness
- A_c is the contact area

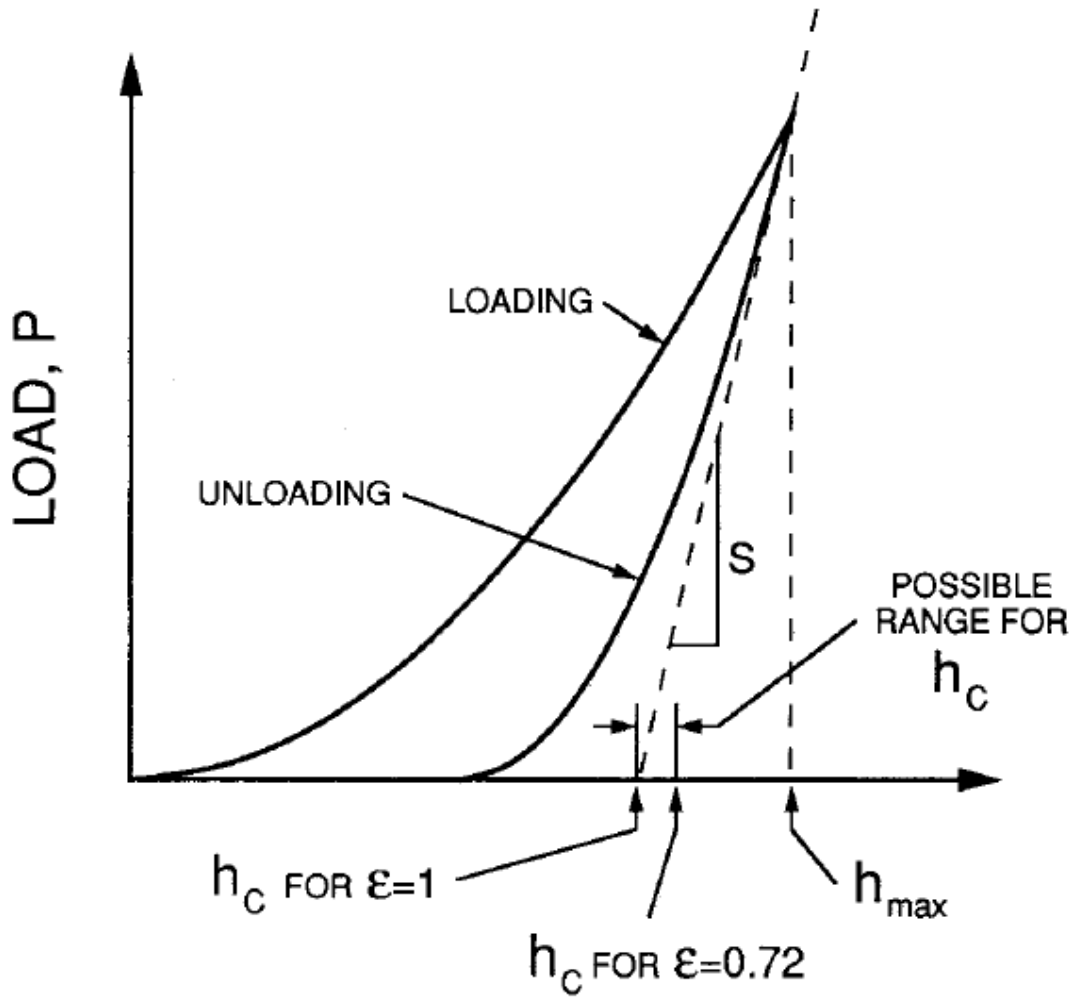

Oliver and Pharr method

- Given that the indenter does not itself deform significantly, the projected contact area at peak load can then be computed from the relation

$$A = F(h_c)$$

- F is the area function which relates the cross-sectional area of the indenter to the distance from its tip

$$h_c = h_{\max} - h_s$$

- Since h_{max} can be experimentally measured, the key to the analysis then becomes how the displacement of the surface at the contact perimeter h_s, can be ascertained from the load-displacement data.

Oliver and Pharr method

- The deflection of the surface at the contact perimeter depends on the indenter geometry

$$h_s = \frac{(\pi - 2)}{\pi}(h - h_f) \qquad h_s = \epsilon \frac{P_{\max}}{S}$$

- the geometric constant ϵ for conical indenter ($\epsilon = 0.72$)

$$\epsilon = \frac{2}{\pi}(\pi - 2)$$

- For the flat punch, $\epsilon = 1$, and for the paraboloid of revolution, $\epsilon = 0.75$

Oliver and Pharr method

$$H = \frac{P_{max}}{A_c}$$

- H is the indentation hardness
- P_{max} is maximum force

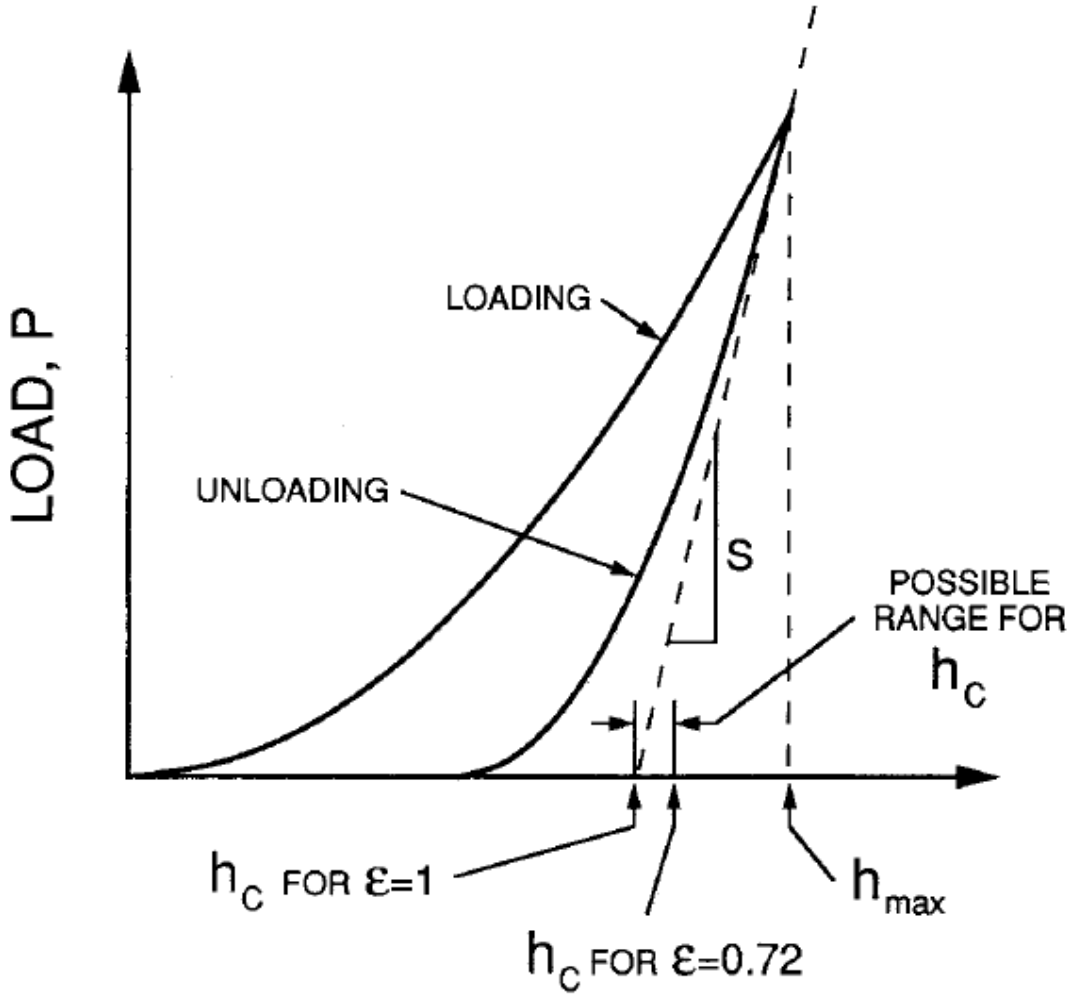

Oliver and Pharr method

- For an ideal indenter

$$A(h_c) = 24.5h_c^2$$

- For a realistic indenter

$$A = \frac{\pi}{4}\frac{1}{E_r^2}\frac{1}{(C - C_f)^2}$$

$$A(h_c) = 24.5h_c^2 + C_1h_c^1 + C_2h_c^{1/2} + C_3h_c^{1/4} + \ldots\ldots\ldots + C_8h_c^{1/128}$$

- C is the total measured compliance
- C_f is the compliance of the load frame

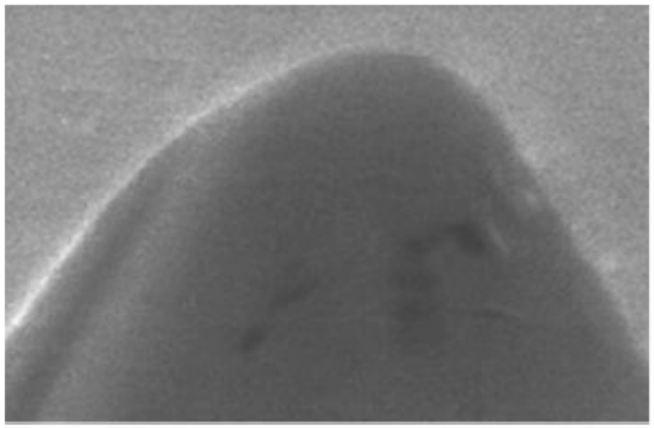

Types of indenter geometries

A. conical

B. Berkovich

C. Vickers

D. Knoop

E. Cube-corner

F. Spherical

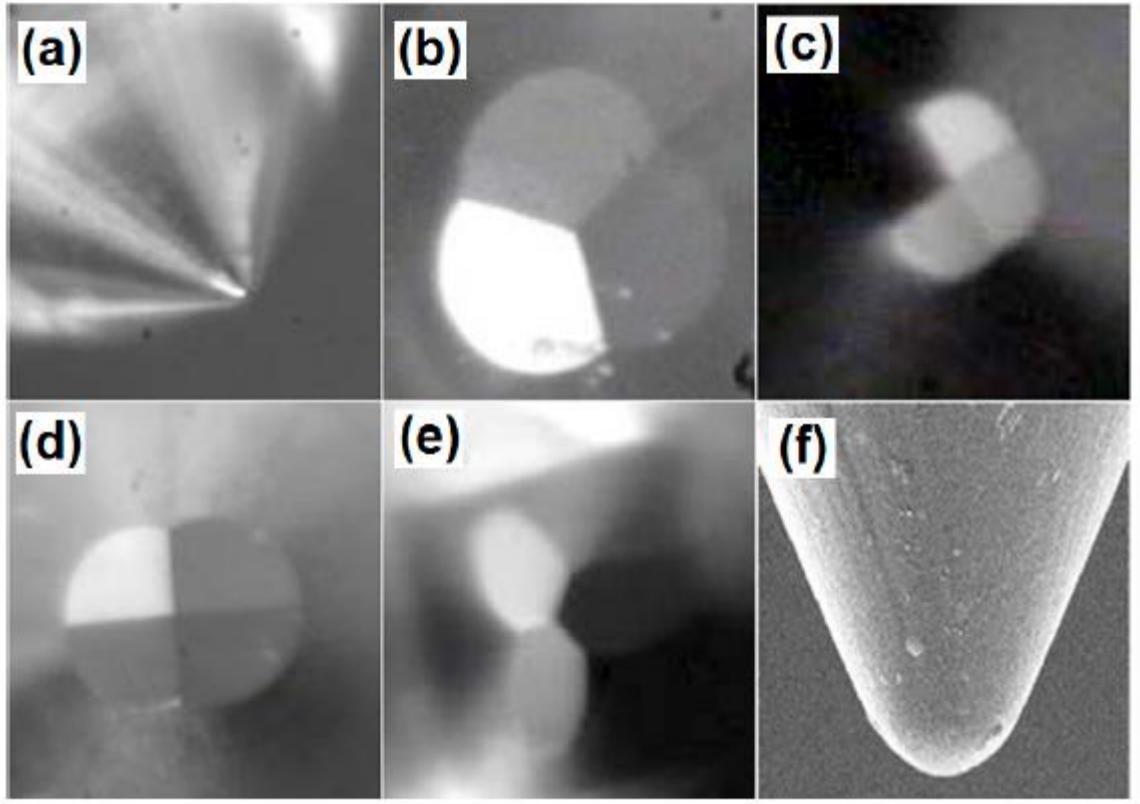

Liu et al., (2017) Progress in Indentation Study of Materials via Both Experimental and Numerical Methods. *Crystals*

Fischer-Cripps (2013) IBIS. *Fischer-Cripps Laboratories*

Conical

- Has a sharp, self-similar geometry. Normally, the cone angle is either 60° or 90°. The conical tip is also normally used for scratch test, wear testing, nano-scale 3D imaging, and tensile and compressive test in nanosetups.

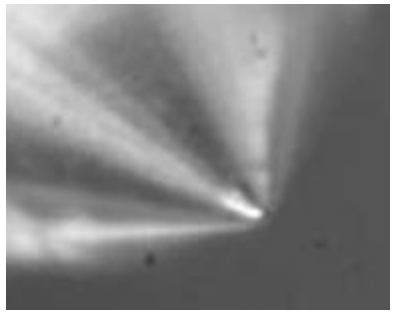

Berkovich

- Three sided pyramid makes easy to maintain its geometry at the micro and nano-scale.
- In theory the cheaper to manufacture
- Used normally for testing bulk material, thin films, polymers, scratch test, wear test, in-situ imaging, and nano tensile and compressive setups

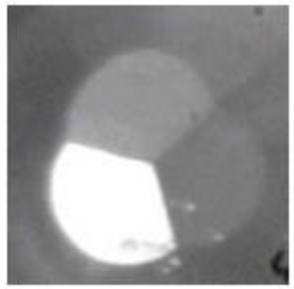

$\theta = 65.27°$

$\alpha = 70.296°$

Ideal Berkovich indenter

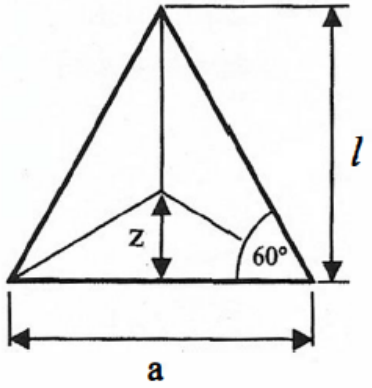

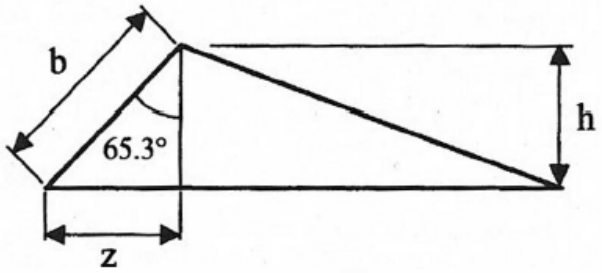

Projected area

$$\tan 60 = \frac{l}{a/2}$$

$$l = \frac{\sqrt{3}}{2}a$$

$$A_{proj} = \frac{al}{2}$$

$$= \frac{\sqrt{3}}{4}a^2 \approx 0.433a^2$$

$$\cos 65.27 = \frac{h}{b}$$

$$h = \frac{a\cos 65.27}{2\sqrt{3}\sin 65.27}$$

$$= \frac{a}{2\sqrt{3}\tan 65.27}$$

$$a = 2\sqrt{3}h\tan 65.27$$

$$A_{proj} = 3\sqrt{3}h^2\tan^2 65.27$$

$$= 24.49h^2$$

Surface area

$$A_{surf} = 3\frac{ab}{2}$$

$$\sin 65.27 = \frac{z}{b}$$

$$z = \frac{a}{2}\tan 30$$

$$= \frac{a}{2\sqrt{3}}$$

$$b = \frac{a}{2\sqrt{3}\sin 65.27}$$

$$A_{surf} = 3\frac{a^2}{4\sqrt{3}\sin 65.27}$$

$$\approx 0.477a^2$$

$$a = 2\sqrt{3}h\tan 65.27$$

$$A_{surf} \approx 26.98h^2$$

Equivalent cone angle:
70.3°

For cube corner, replace 65.27° with 35.264°

Equivalent cone angle: 42.28°

For original Berkovich indenter, 65.0333°

$A_{proj} = 23.97h^2$

$A_{surf} = 26.40h^2$

Vickers

- Four sided pyramid and suitable for measuring mechanical properties at a really small scale.
- Line of conjunction at tip limits the sharpness of tip for the determination of hardness for very shallow indents.
- Used normally to test bulk material, films and foils, scratch test, and wear tests.

$\theta = 68°$

$\alpha = 70.3°$

Knoop

- Originally design for hard metals
- Used to probe anisotropy in surface of samples

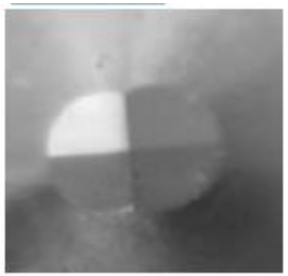

$\theta_1 = 86.25°, \theta_2 = 65°$

$\alpha = 77.64°$

Cube-corner

- Three-sided pyramid with mutually perpendicular faces, which is like a corner of a cube. Design to provide great amount of deformation for fracture toughness determination from induced cracks. The toughness at the microscale or nanoscale can be investigated via the induced cracks. Nevertheless, a very fragile and easily broken tip.

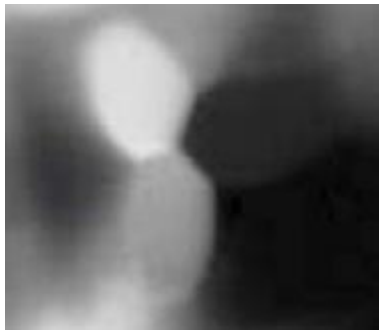

$\theta = 35.26°$

$\alpha = 42.278°$

Spherical

- Can be used to examine yielding and work hardening. This works like, the contact stresses with spherical indenters are initially small and produce only elastic deformation, with increasing indentation depth, a transition from elastic to plastic deformation can be captured.

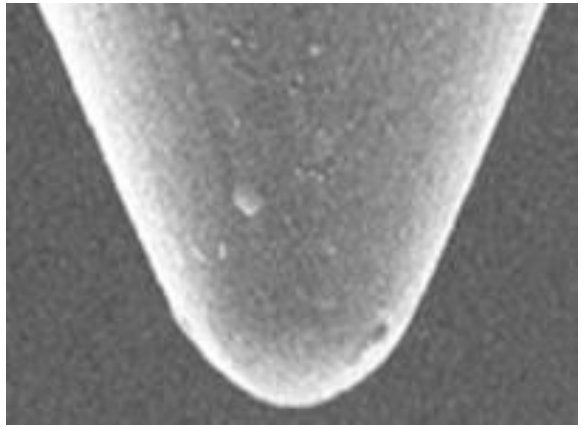

Control methods for nanoindentation

- Load controlled
- Displacement controlled
- Open-loop

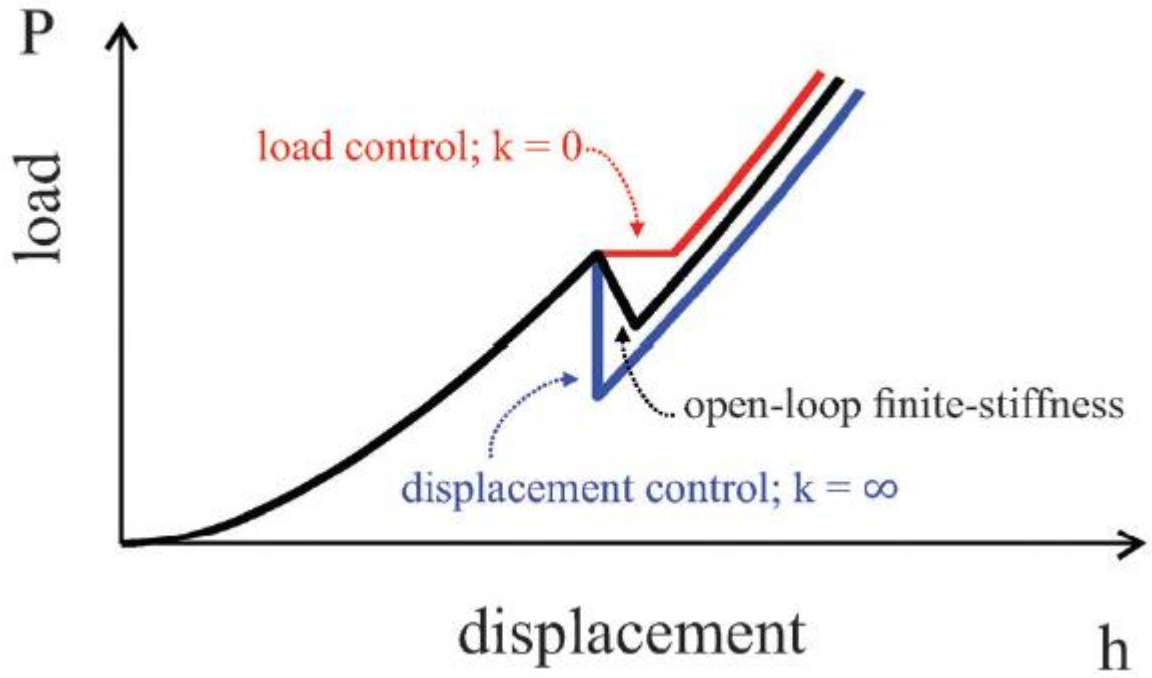

Paul, D Oliver, P Grütter (2014) Indentation-formed nanocontacts: an atomic-scale perspective, *Phys. Chem. Chem. Phys.,*16, 8201-8222

Creep affecting results

Sun, Y., Liang, J., Xu, ZH. et al. (2008) Nanoindentation for measuring individual phase mechanical properties of lead free solder alloy. *J Mater Sci: Mater Electron* 19, 514–521.

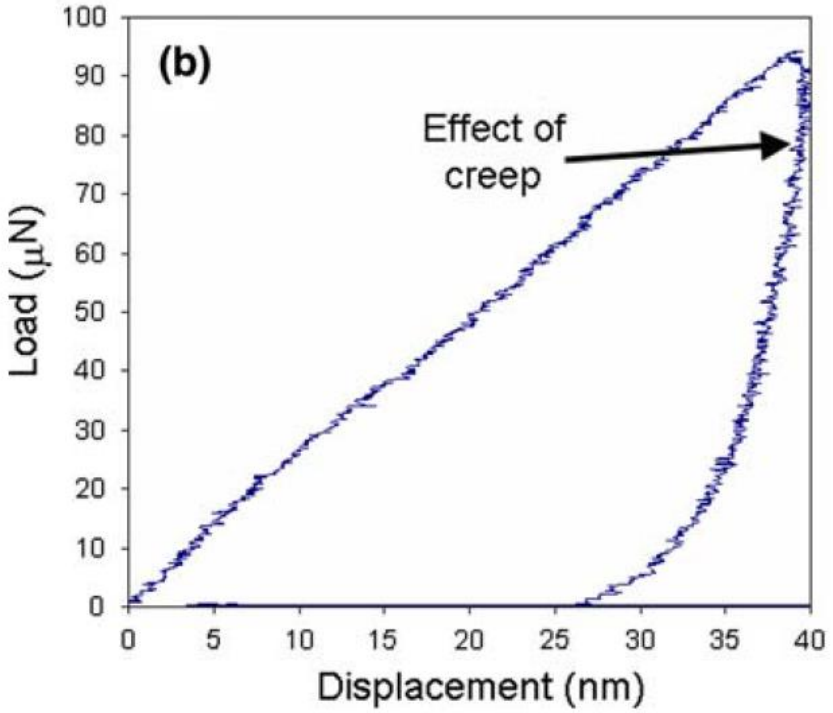

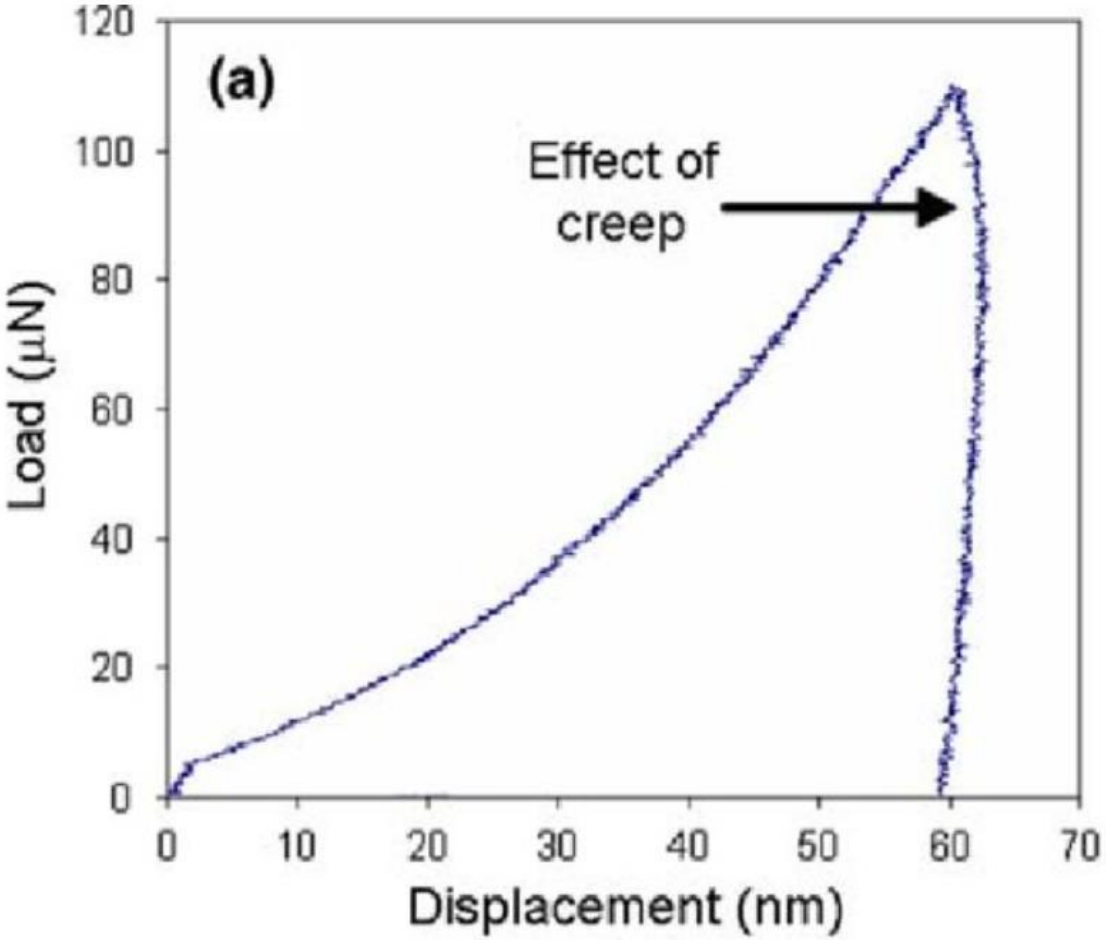

Trapezoidal loading-unloading

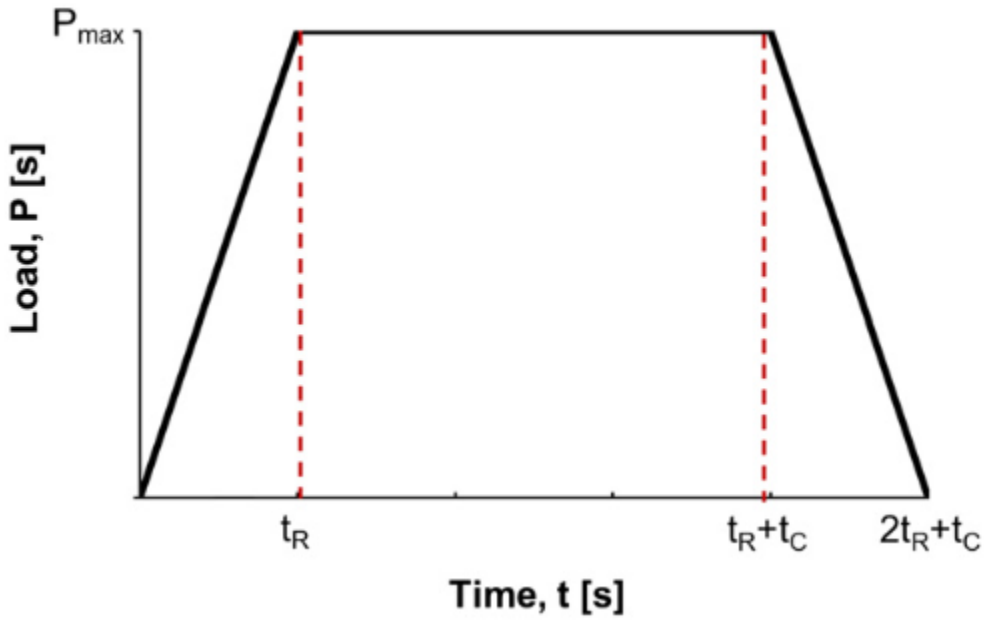

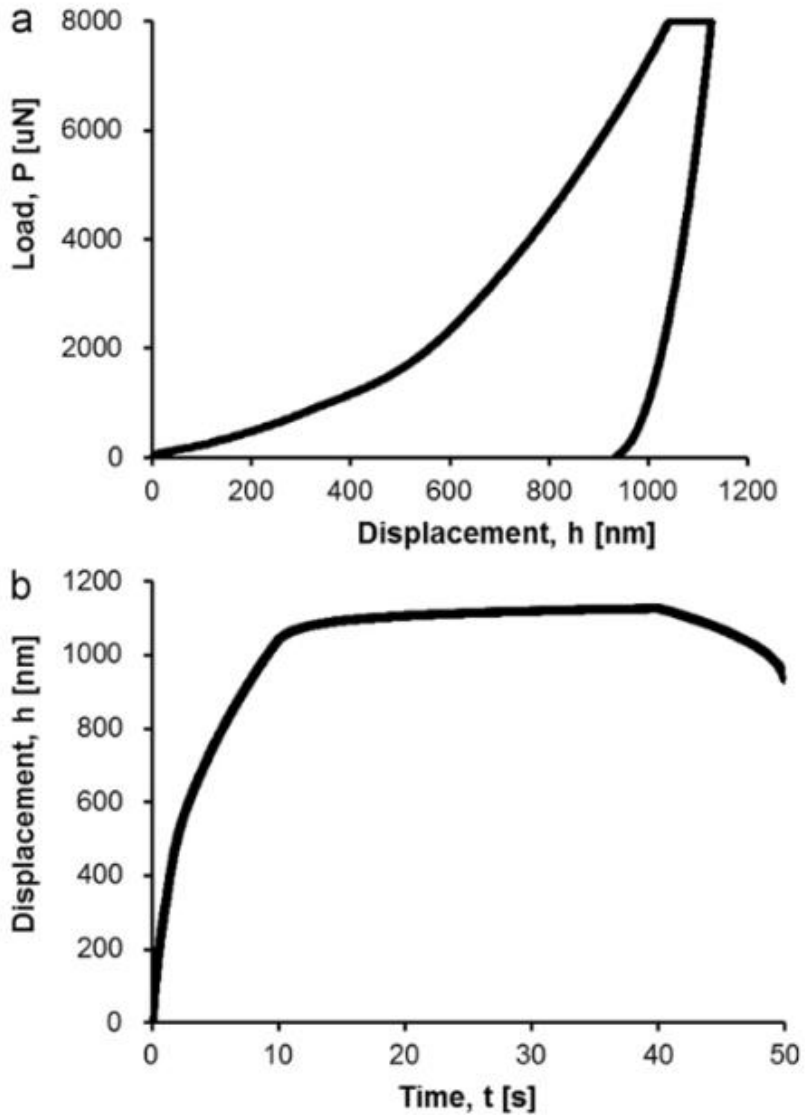

Naiara Rodriguez-Florez, Michelle L. Oyen, Sandra J. Shefelbine, (2013) Insight into differences in nanoindentation properties of bone, Journal of the Mechanical Behavior of Biomedical Materials, Volume 18

Nanoindentation on cortical bone

Casanova M, Balmelli A, Carnelli D, Courty D, Schneider P, Müller R. (2017) Nanoindentation analysis of the micromechanical anisotropy in mouse cortical bone. *R. Soc. open sci*. 4: 160971

GOAL: Anisotropy of bone

LOCATION: proximal, central and distal of the shaft from femora

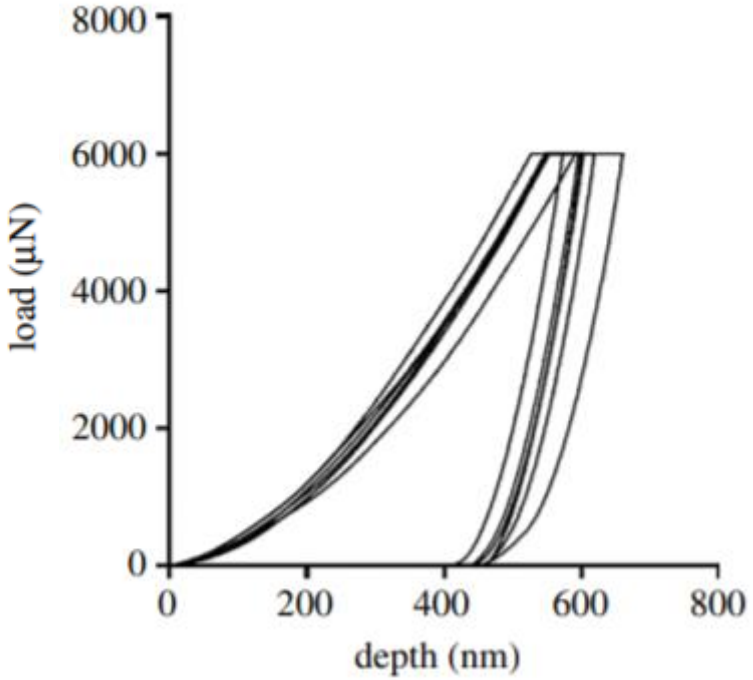

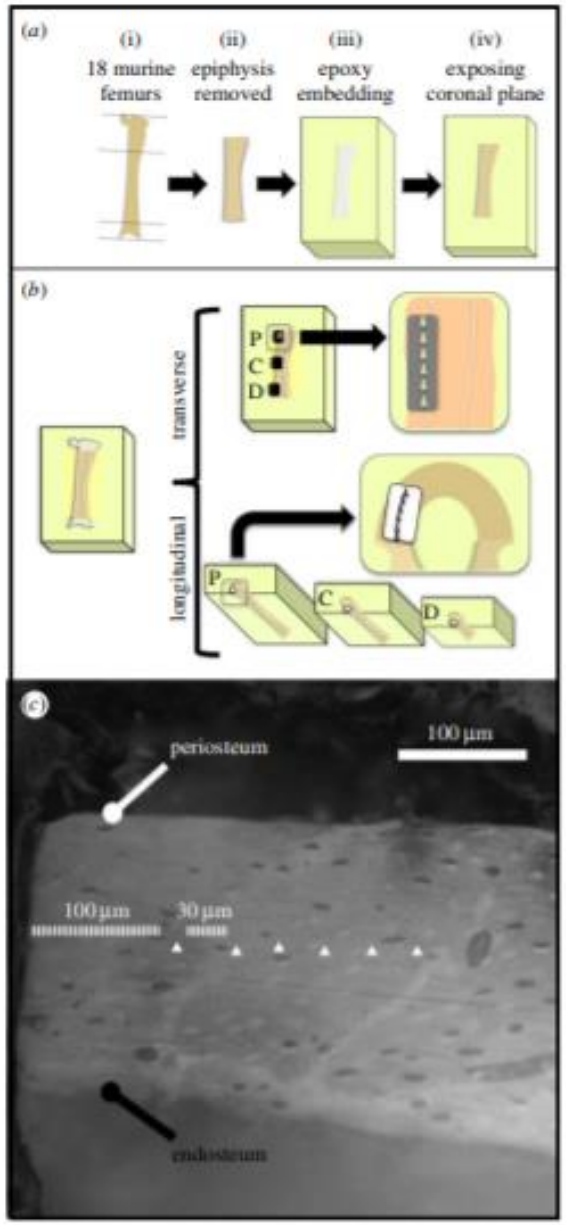

Nanoindentation on cortical bone

Casanova M, Balmelli A, Carnelli D, Courty D, Schneider P, Müller R. (2017) Nanoindentation analysis of the micromechanical anisotropy in mouse cortical bone. *R. Soc. open sci*. 4: 160971

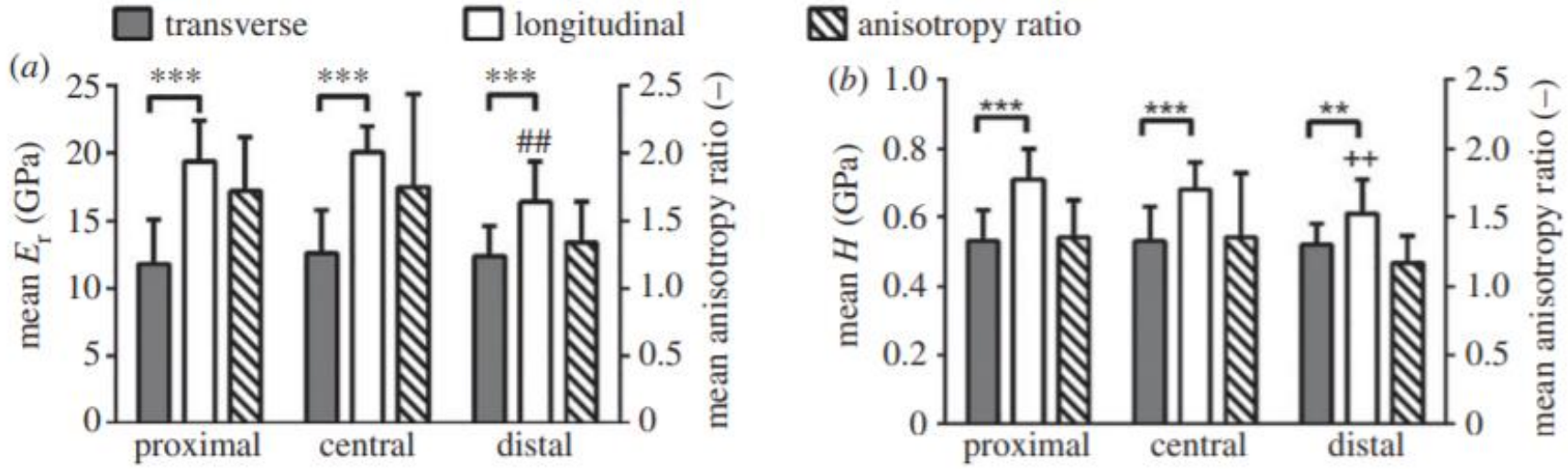

Nanoindentation on cortical bone

Furin, I., Pastrama, M., Kariem, H., Luczynski, K., Lahayne, O., & Hellmich, C. (2016). A New Nanoindentation Protocol for Identifying the Elasticity of Undamaged Extracellular Bone Tissue. MRS Advances, 1(11)

Statistical Nanoindentation

- Developed at the MIT for cementitious materials
- Distinguish undamaged and unaffected ECBM

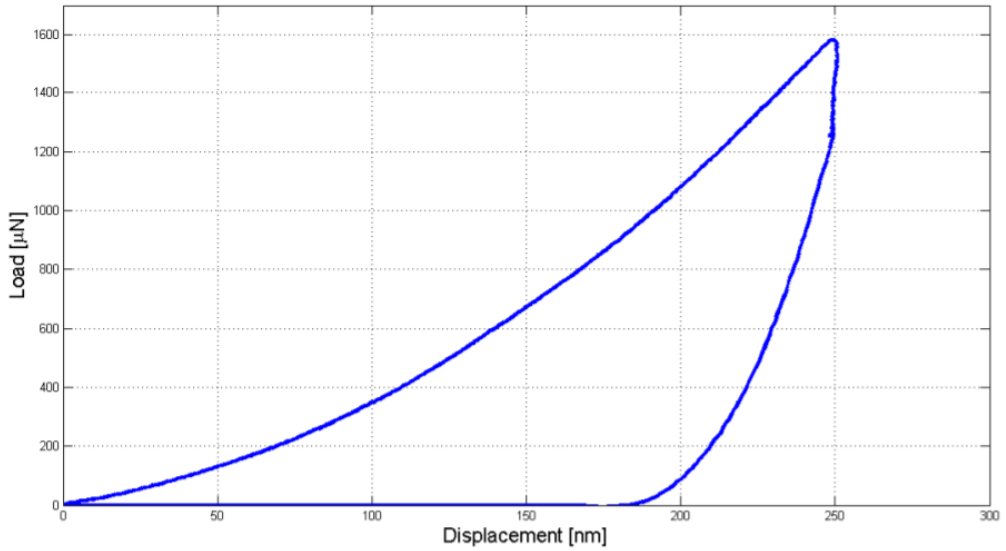

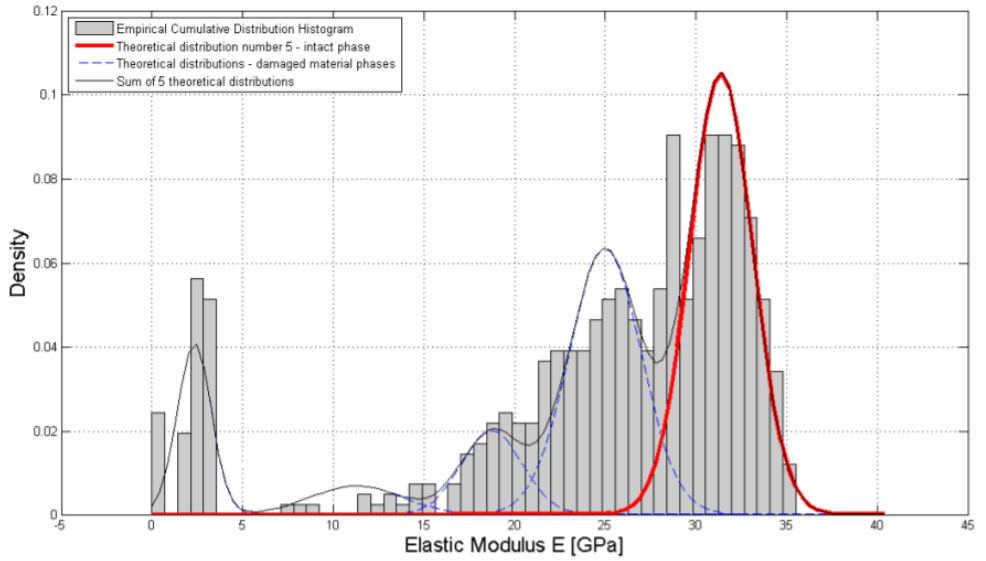

Nanoindentation on cortical bone

Furin, I., Pastrama, M., Kariem, H., Luczynski, K., Lahayne, O., & Hellmich, C. (2016). A New Nanoindentation Protocol for Identifying the Elasticity of Undamaged Extracellular Bone Tissue. MRS Advances, 1(11)

- Lower Elastic modulus is related to micro cracks and porosity

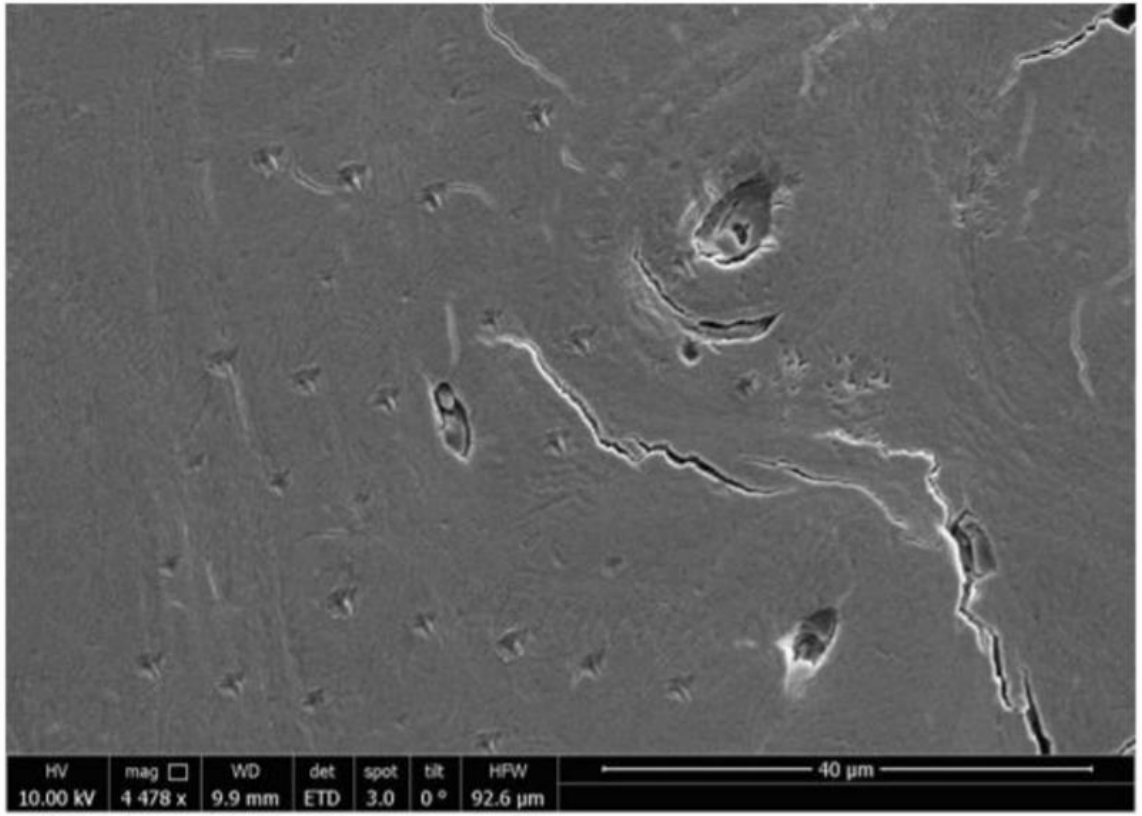

Microcracks in bone

- Microcracks are present in bone and can result from fatigue damage due to repeated, cyclically applied stresses.
- From a mechanical-point, microcracks can dissipate strain energy at the advancing tip of a crack to improve overall bone toughness.
- Physiologically, microcracks are thought to trigger bone remodeling.

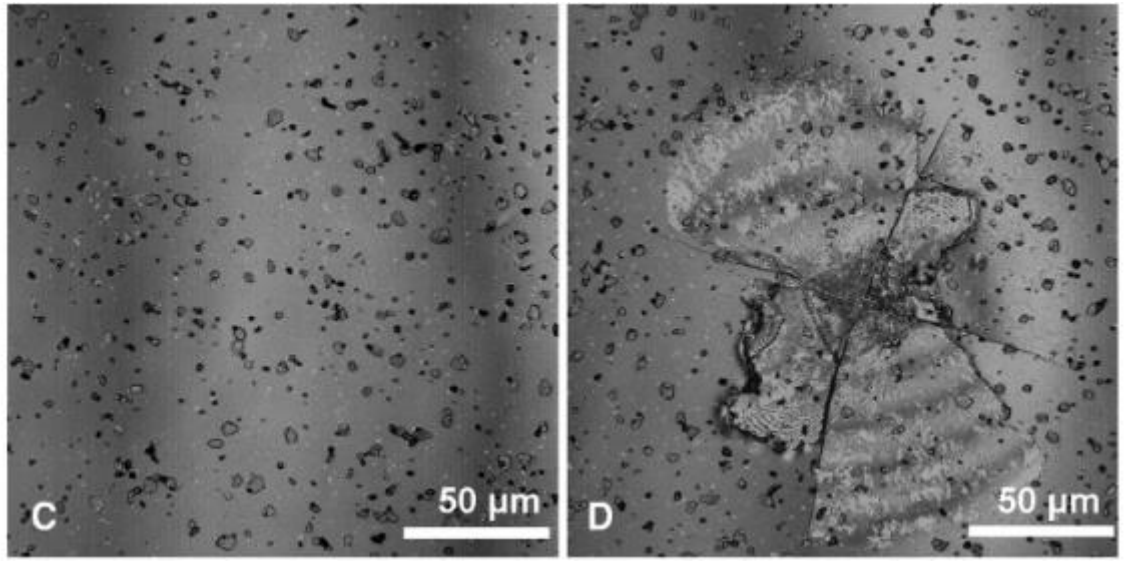

Microcracks in bone

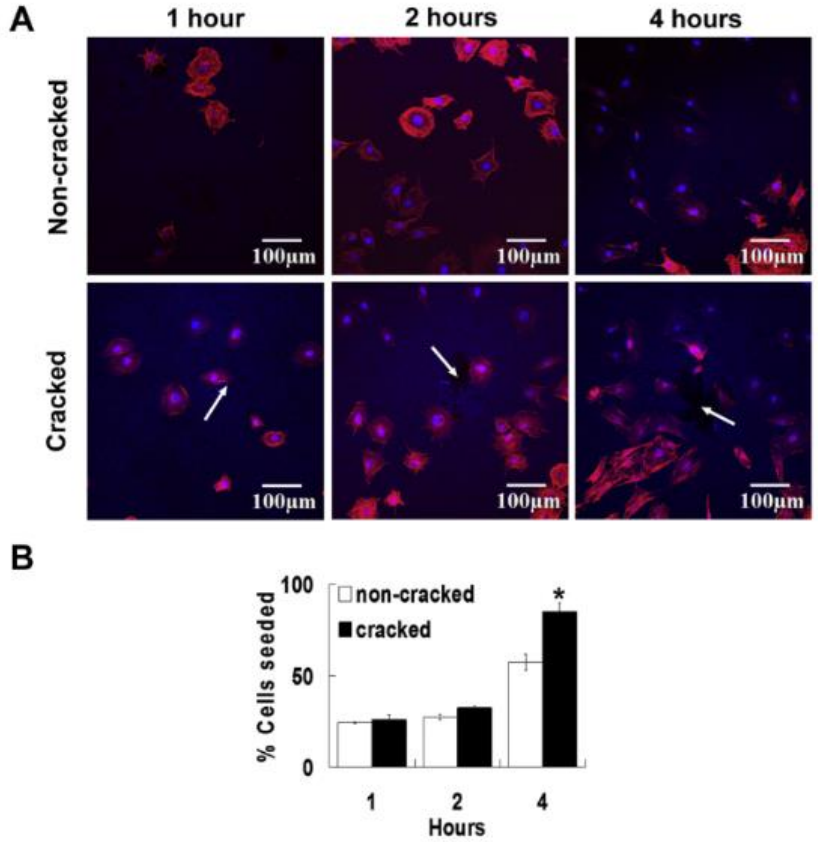

Yutian Shu, Melissa J. Baumann, Eldon D. Case, Regina K. Irwin, Sarah E. Meyer, Craig S. Pearson, Laura R. McCabe (2014) Surface microcracks signal osteoblasts to regulate alignment and bone formation, *Materials Science and Engineering: C*, Volume 44

Wolff's Law

- In the late 19th century, German surgeon Julius Wolff described bone remodeling and how it relates to the stress placed on bones. According to Wolff, bones will adapt according to the demands placed on them.

- The premise that bones grow and remodel throughout life to adapt to their mechanical environment is often called Wolff's law.

- However, is not always true, and in fact comprises a variety of different processes that are best considered separately.

Pearson OM, Lieberman DE. (2004) The aging of Wolff's "law": ontogeny and responses to mechanical loading in cortical bone. *Am J Phys Anthropol*

Micropillar compressive test in bone

Schwiedrzik, J., Raghavan, R., Bürki, A. *et al.* (2014) *In situ* micropillar compression reveals superior strength and ductility but an absence of damage in lamellar bone. *Nature Mater* **13,** 740–747

- isolated lamellae exhibit a plastic behavior, with higher yield stress and ductility but no damage

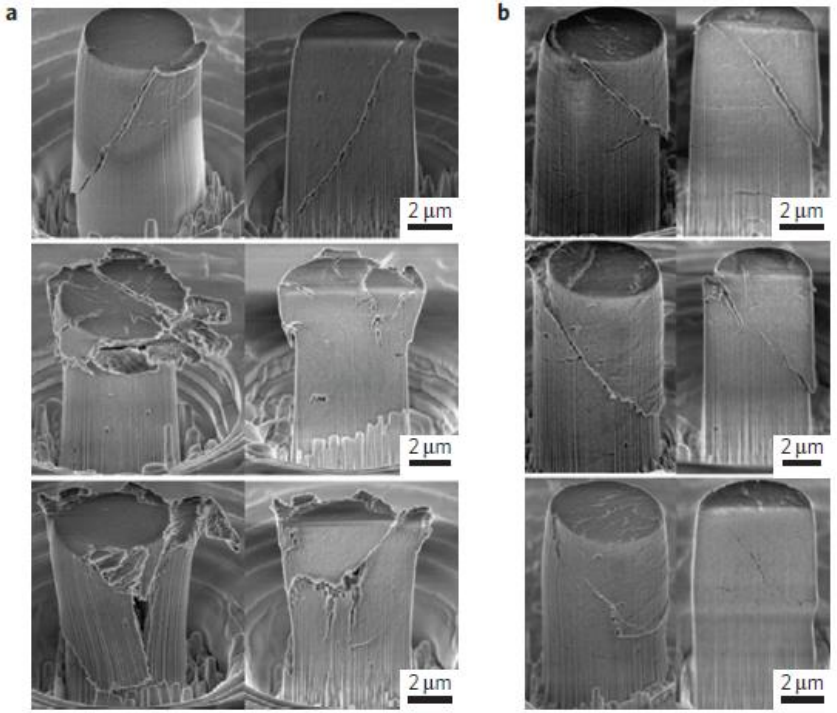

Micropillar compressive test in bone

Schwiedrzik, J., Raghavan, R., Bürki, A. *et al.* (2014) *In situ* micropillar compression reveals superior strength and ductility but an absence of damage in lamellar bone. *Nature Mater* **13,** 740–747

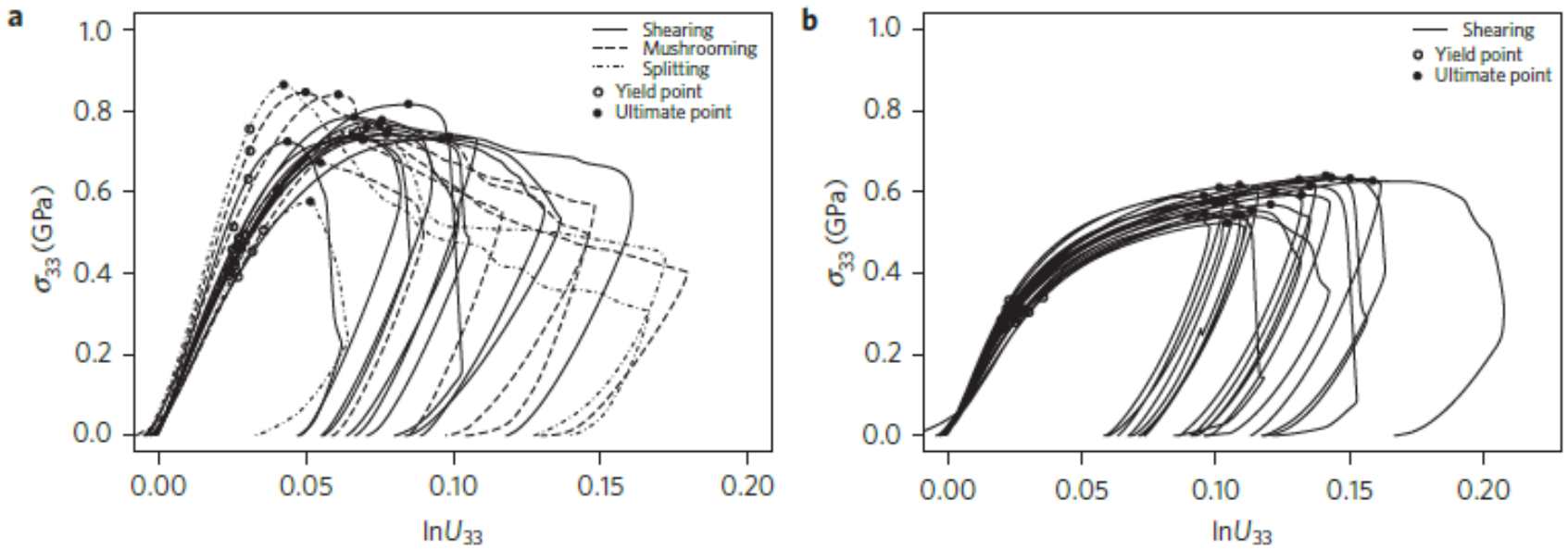

Micropillar compressive test in bone

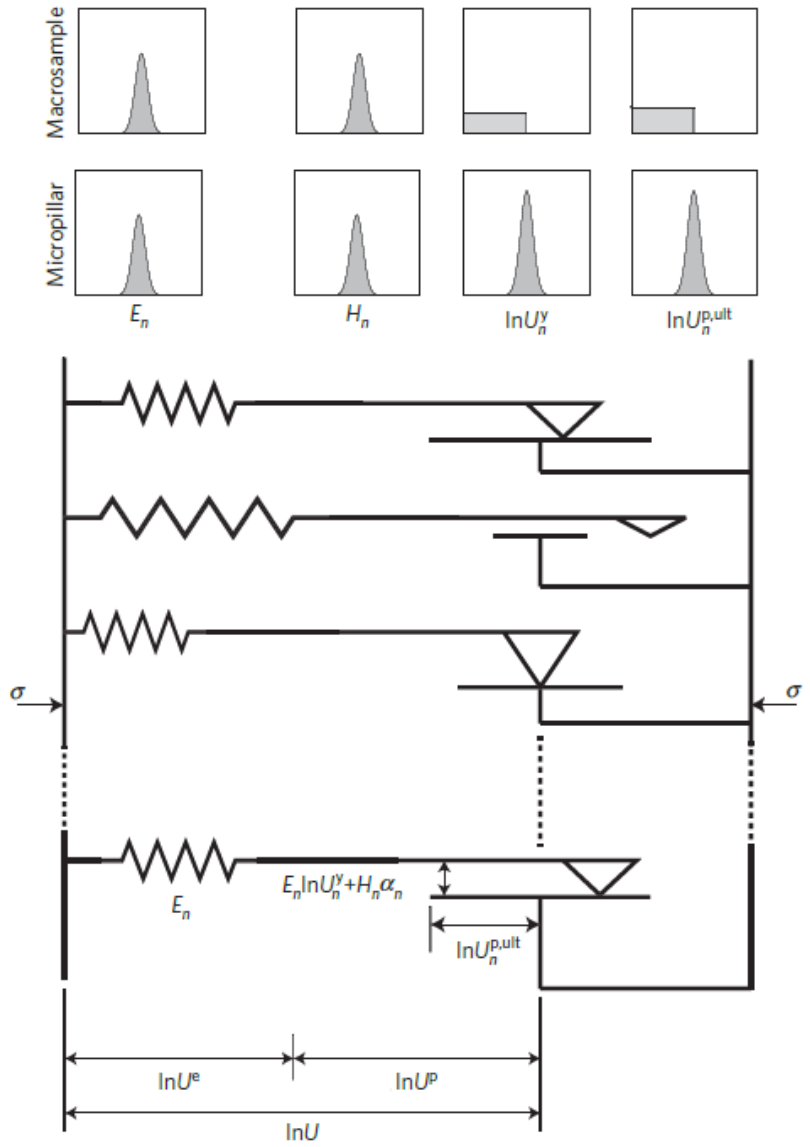

Rheological model describing the mechanical response of bone under compression

- A parallel array of elastic springs in series with plastic pads failing at an ultimate plastic strain under compressive stress

Schwiedrzik, J., Raghavan, R., Bürki, A. *et al.* (2014) *In situ* micropillar compression reveals superior strength and ductility but an absence of damage in lamellar bone. *Nature Mater* **13,** 740–747

Micropillar compressive test in bone

Krzysztof W. Luczynski, Andreas Steiger-Thirsfeld, Johannes Bernardi, Josef Eberhardsteiner, Christian Hellmich (2015) Extracellular bone matrix exhibits hardening elastoplasticity and more than double cortical strength: Evidence from homogeneous compression of non-tapered single micron-sized pillars welded to a rigid substrate, *Journal of the Mechanical Behavior of Biomedical Materials*, Volume 52

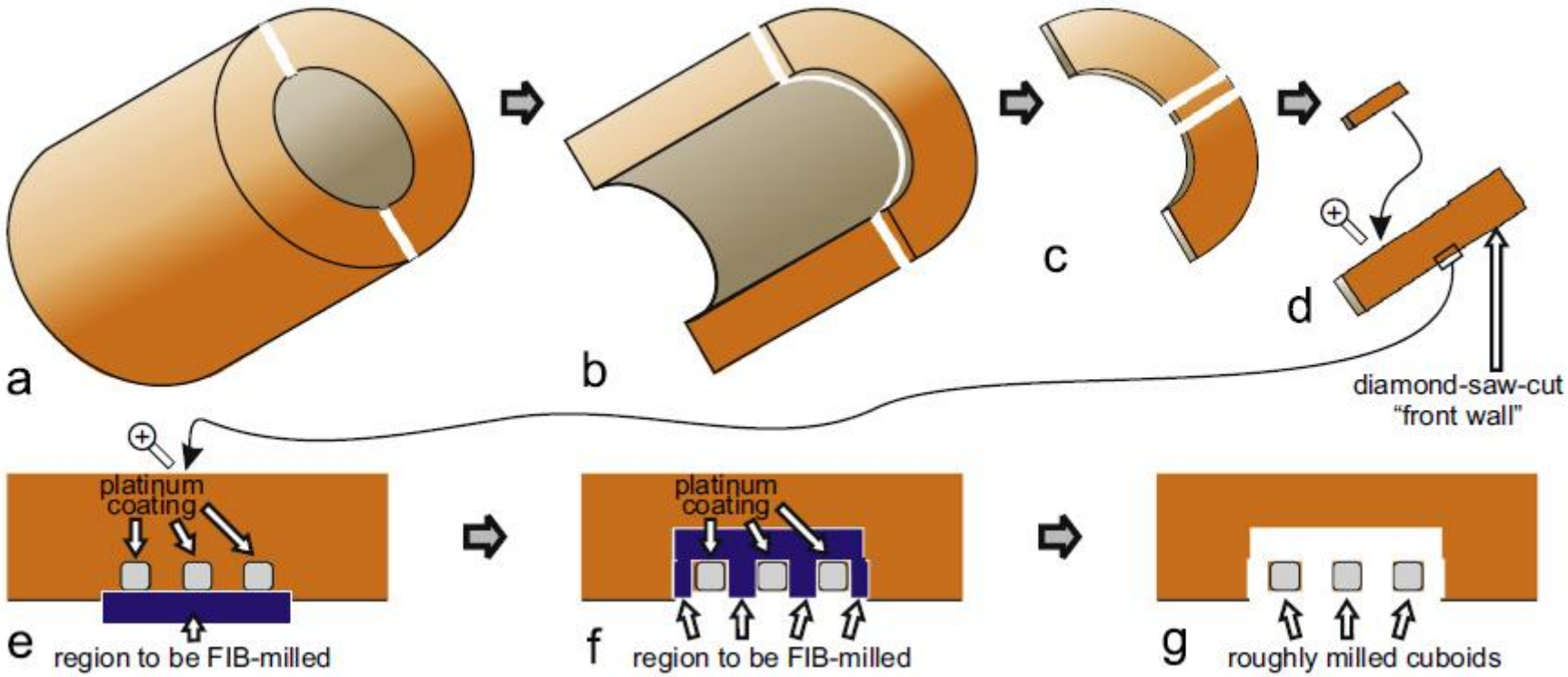

Micropillar compressive test in bone

Krzysztof W. Luczynski, Andreas Steiger-Thirsfeld, Johannes Bernardi, Josef Eberhardsteiner, Christian Hellmich (2015) Extracellular bone matrix exhibits hardening elastoplasticity and more than double cortical strength: Evidence from homogeneous compression of non-tapered single micron-sized pillars welded to a rigid substrate, *Journal of the Mechanical Behavior of Biomedical Materials*, Volume 52

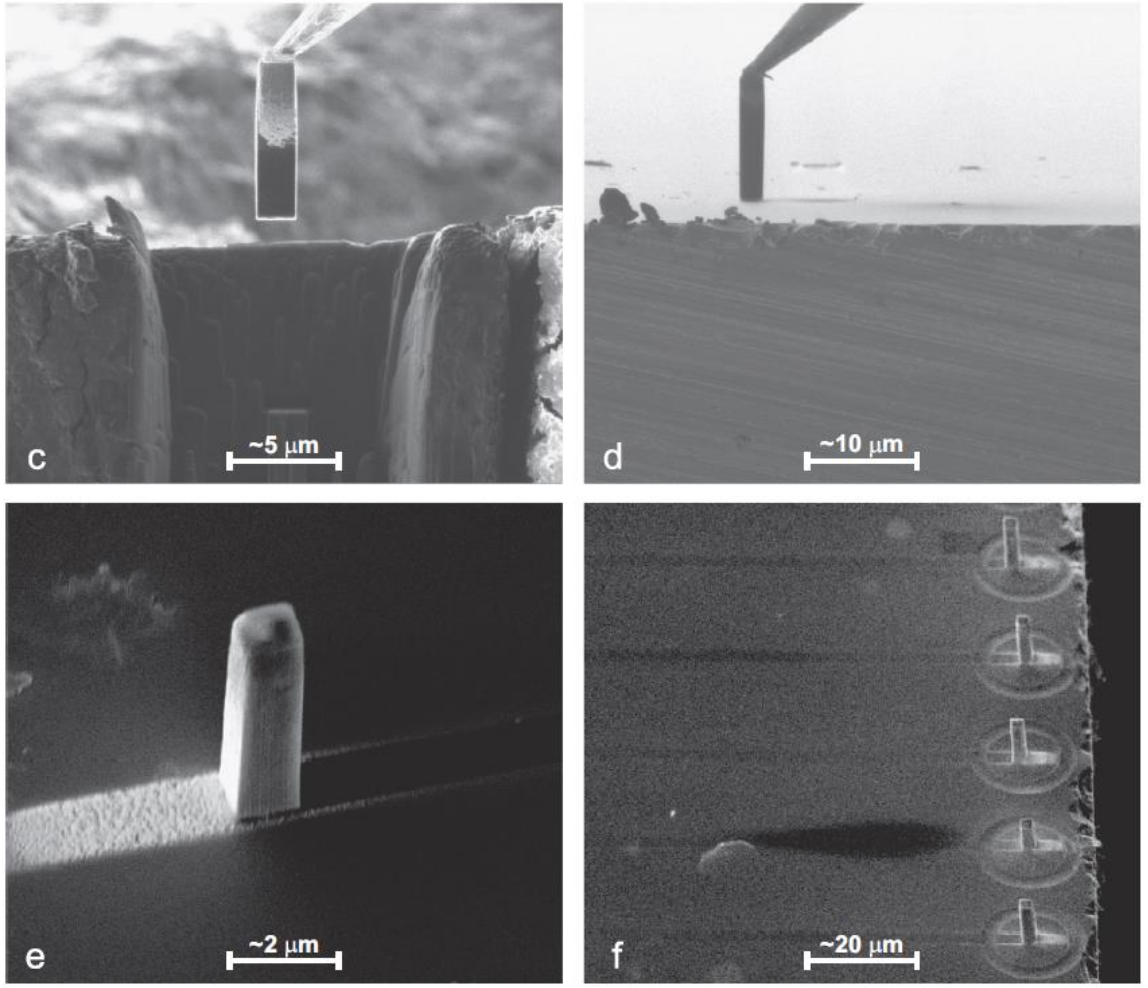

Micropillar compressive test in bone

Krzysztof W. Luczynski, Andreas Steiger-Thirsfeld, Johannes Bernardi, Josef Eberhardsteiner, Christian Hellmich (2015) Extracellular bone matrix exhibits hardening elastoplasticity and more than double cortical strength: Evidence from homogeneous compression of non-tapered single micron-sized pillars welded to a rigid substrate, *Journal of the Mechanical Behavior of Biomedical Materials*, Volume 52

- Uniaxial strength turns out as at least twice that measured macroscopically, and respective ultimate stresses are preceded by hardening elastoplastic states, already at very low load levels.

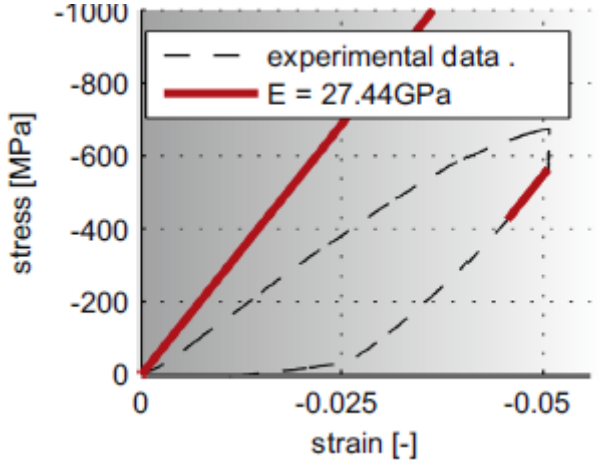

Micropillar compressive test in bone

Krzysztof W. Luczynski, Andreas Steiger-Thirsfeld, Johannes Bernardi, Josef Eberhardsteiner, Christian Hellmich (2015) Extracellular bone matrix exhibits hardening elastoplasticity and more than double cortical strength: Evidence from homogeneous compression of non-tapered single micron-sized pillars welded to a rigid substrate, *Journal of the Mechanical Behavior of Biomedical Materials*, Volume 52

- From the beginning of the loading phase, more work is put into the system than would ever be recovered upon unloading – hence, the entire loading branch is of elastoplastic nature
- The work recovered during unloading, on the other hand, gives access to the elastic energy which has been stored within the sample during the loading phase

Ultrasound test

- Elasticity determination through ultrasonic test has been applied to a wide range of materials

$$\rho_{\text{app}} = \frac{M}{V}$$

$$\mathrm{v}_i = \frac{\ell_{\mathrm{s}}}{t_{\mathrm{s}}}$$

- Longitudinal (compressional) and transversal (shear) [V_l and V_T]
- Distance through the specimen ℓ_s

$$\lambda = \frac{\mathrm{v}}{f}$$

- Frequency f wave velocity v and wavelength λ

Ultrasound test

$$C_{1111} = \rho \cdot v_L^2 \quad \text{and} \quad C_{1212} = G = \rho \cdot v_T^2,$$

- are the elastic stiffness tensor components related to normal and shear deformation

$$E = \rho \cdot \frac{v_T^2(3v_L^2 - 4v_T^2)}{v_L^2 - v_T^2} \quad \text{and} \quad \nu = \frac{v_L^2/2 - v_T^2}{v_L^2 - v_T^2},$$

- Young's modulus and Poisson's ratio

Kohlhauser et al., (2009) Ultrasonic Characterization of Porous Biomaterials Across Different Frequencies. *Strain*

Ultrasound test relationship to continuum micromechanics

- the characteristic length of the RVE ℓ_{RVE} needs to be much smaller than the scale of the characteristic loading of the medium, here the wavelength λ

$$d \ll \ell_{\mathrm{RVE}} \ll \lambda$$

Kohlhauser et al., (2009) Ultrasonic Characterization of Porous Biomaterials Across Different Frequencies. *Strain*

Separation of scales

- Natural materials with heterogeneous properties at the microscopic level, but homogenous at the macroscopic scale.

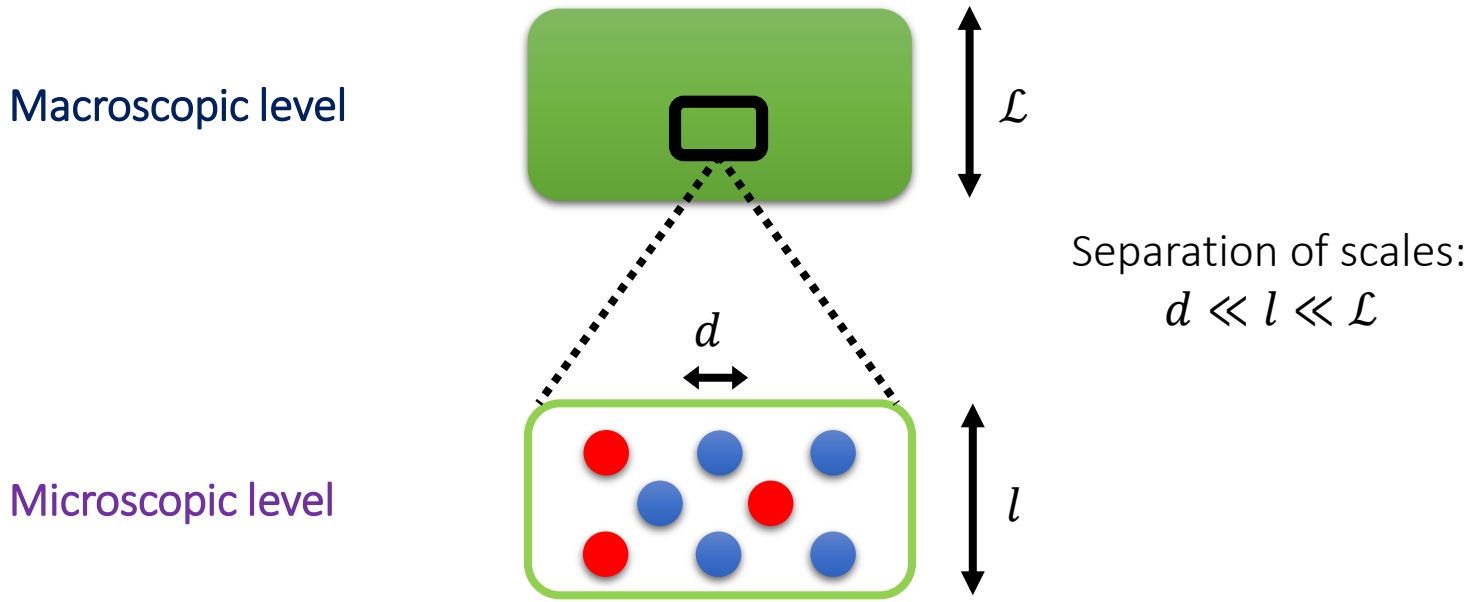

Separation of scales:

$$d \ll l \ll \mathcal{L}$$

Ultrasound test

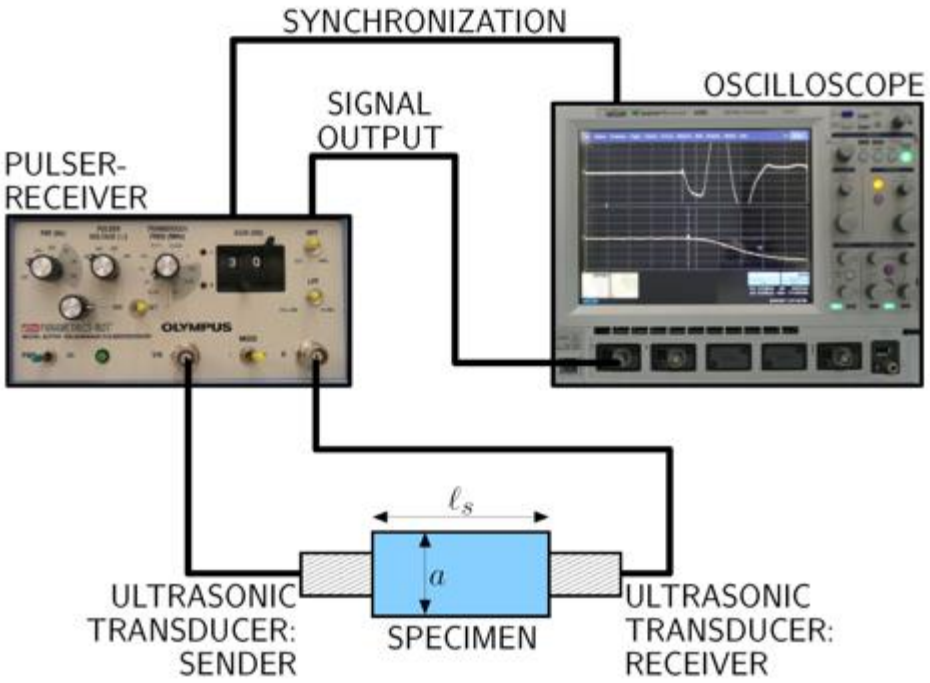

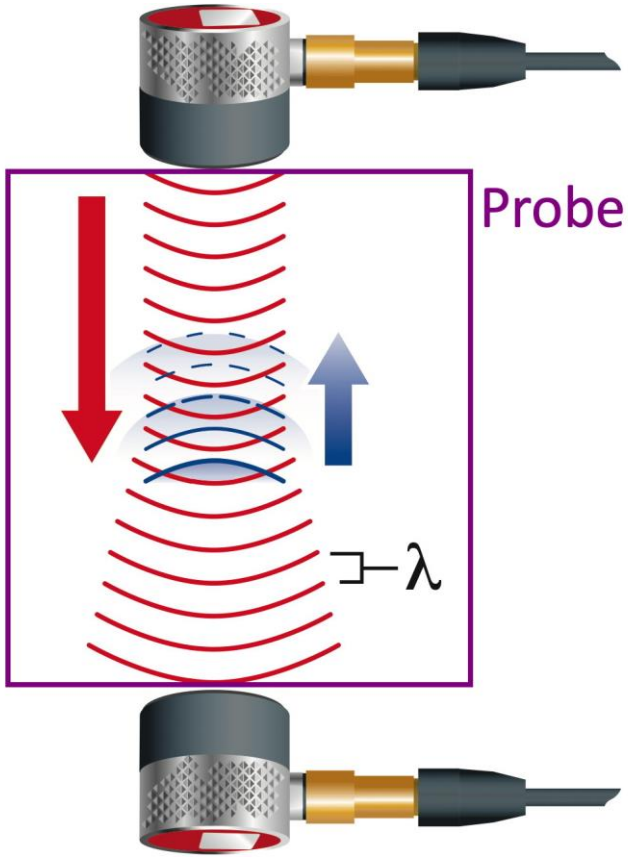

Ultrasound test

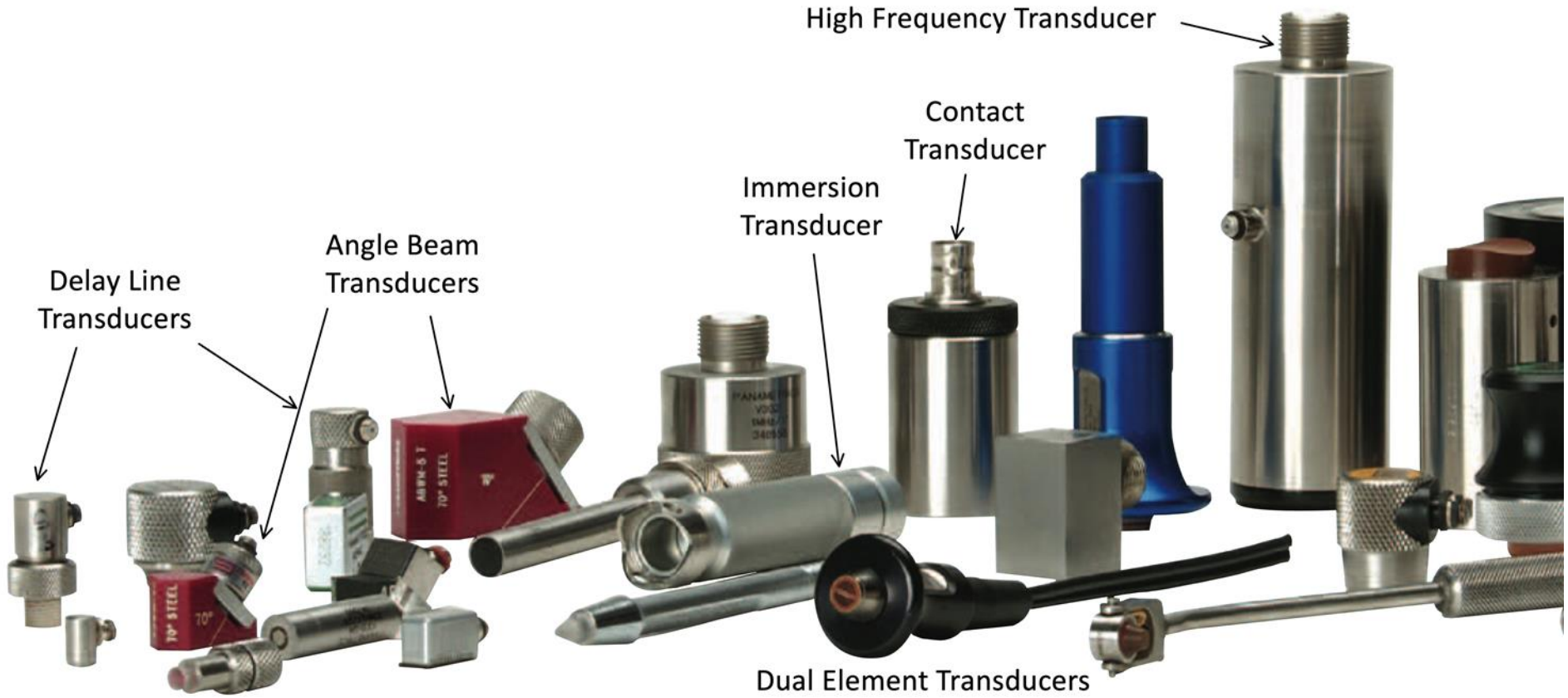

- For more information please take lecture 202.044 Experimental Methods for Analysis of Deformations with Dr. Lahayne.

Electron Microscopy

- Electron microscopy is a recognized standard tool for nanomaterial characterization

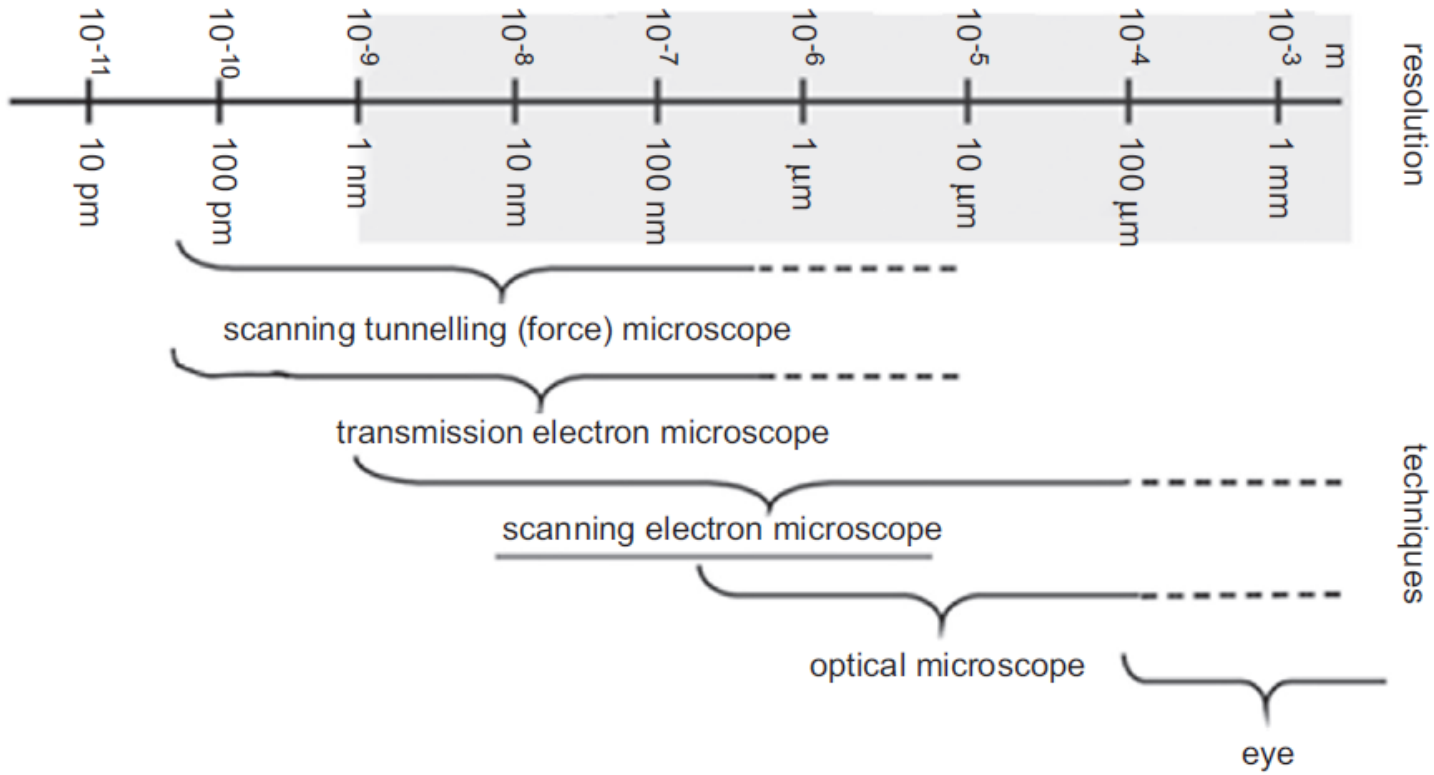

Electron Microscopy

- Types:
  - Transmission electron microscope (TEM)
  - Scanning electron microscope (SEM)
  - Reflection electron microscope (REM)
  - Scanning transmission electron microscope (STEM)
  - Scanning tunneling microscopy (STM)

TEM

- Transmission electron microscopy (TEM) are microscopes that use a particle beam of electrons to visualize specimens and generate a highly-magnified image. TEM comprises all forms of diffraction, imaging, or spectroscopy performed with high-energy electrons in transmission geometry. Electrons are transmitted through a specimen to form an image.

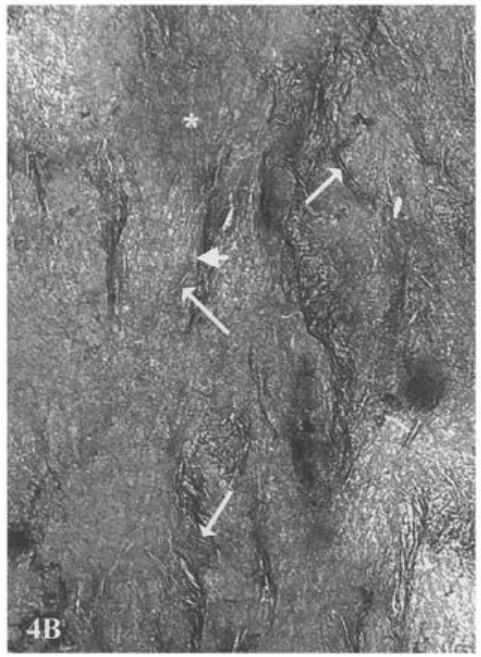

Prostak KS, Lees S. (1996) Visualization of crystal-matrix structure. In situ demineralization of mineralized turkey leg tendon and bone. Calcif Tissue Int.

SEM

- Scanning electron microscopy (SEM) is probably one of the most versatile tools for the analysis of micro- and nanostructures with a wide range of applications. SEM techniques provide information on the topography and composition of surfaces by the collection and processing of signals that are generated by a sharp electron probe within a certain interaction volume.
- energy-dispersive X-ray microanalysis (EDX): elemental analysis by electron-induced X-ray emission

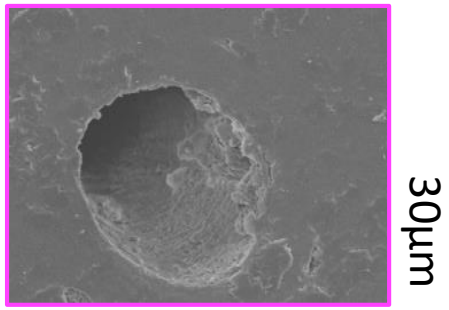

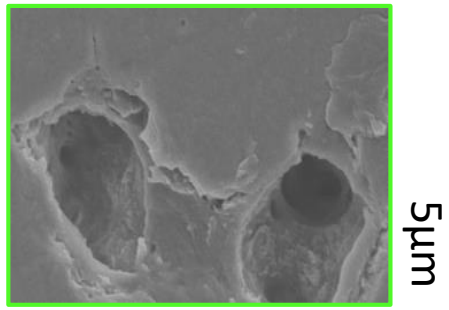

Zelaya-Lainez et al.,(2020) “Variances” and “in-variances” in hierarchical porosity and composition, across femoral tissues from cow, horse, ostrich, emu, pig, rabbit, and frog. *Materials Science and Engineering: C*

REM

- REM is a combination of imaging, diffraction, and spectroscopy techniques for characterization of topography. This type of electron microscope uses scattered electrons that reflect from the surface of the specimen to produce an image.

STEM

- Considered a high resolution version of the SEM, the scanning transmission electron microscope (STEM) focuses on a narrow spot and produces image by scanning the sample in a raster.

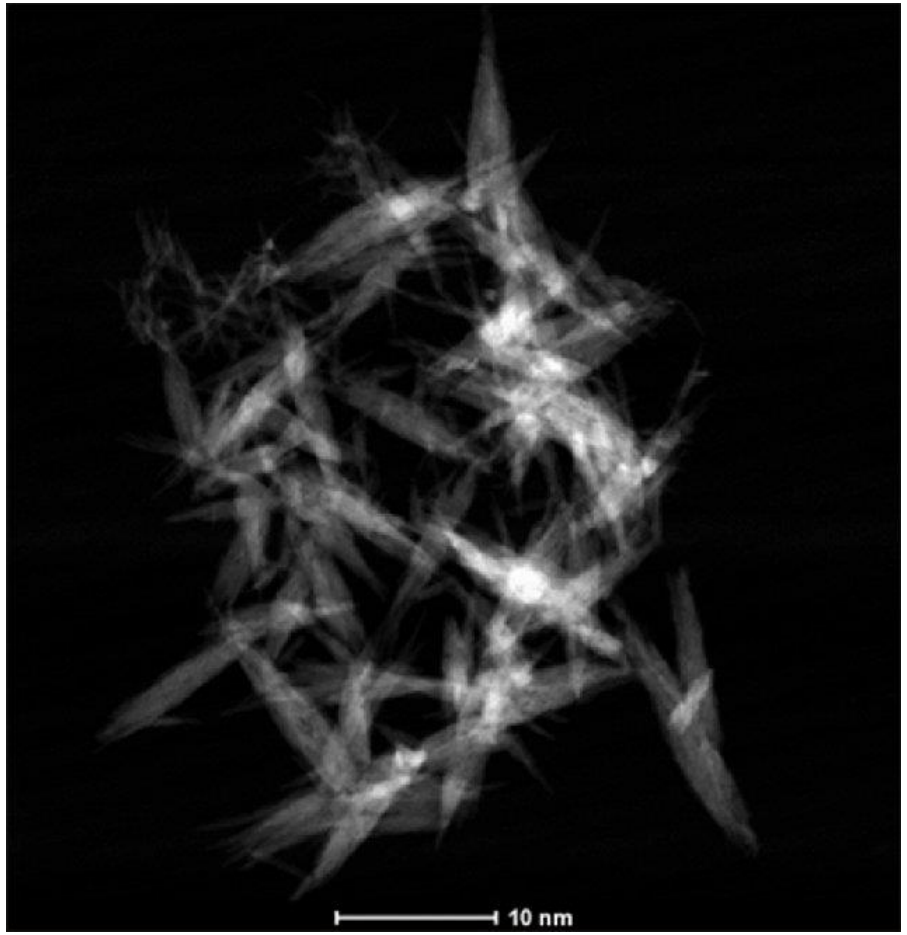

Nadezhdin et al., (2018) Osteogenic properties of new porous composite materials based on titanium with bioactive Covering.
Drug Invention Today

STM

- is a type of microscope used for imaging surfaces at the atomic level. STM works by scanning a very sharp metal wire tip over a surface.

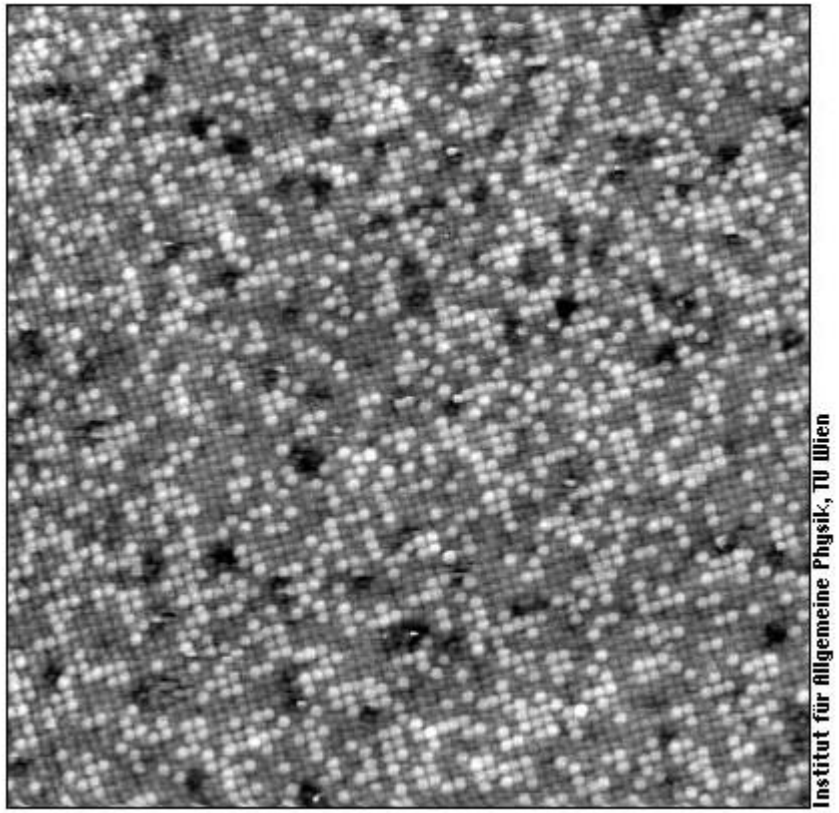

chemical contrast on PtRh(100)
Platinum-Rhodium (100)

Atomic Force Microscope (AFM)

- is one of the most powerful techniques to investigate the status of surface conditions of materials.

- Three abilities:
  - Force measurement
  - Topography
  - Manipulation of sample

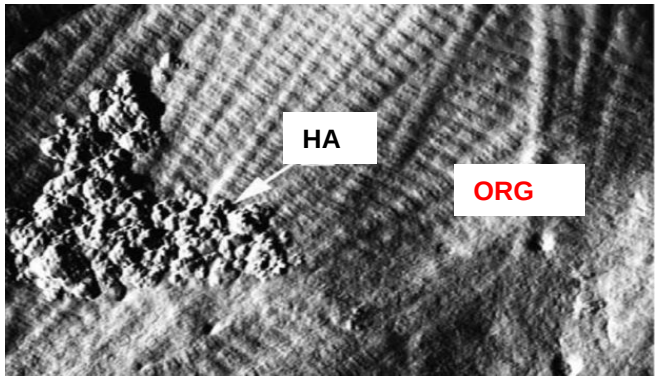

Hassenkam et al., 2005, *Micron*, 36.

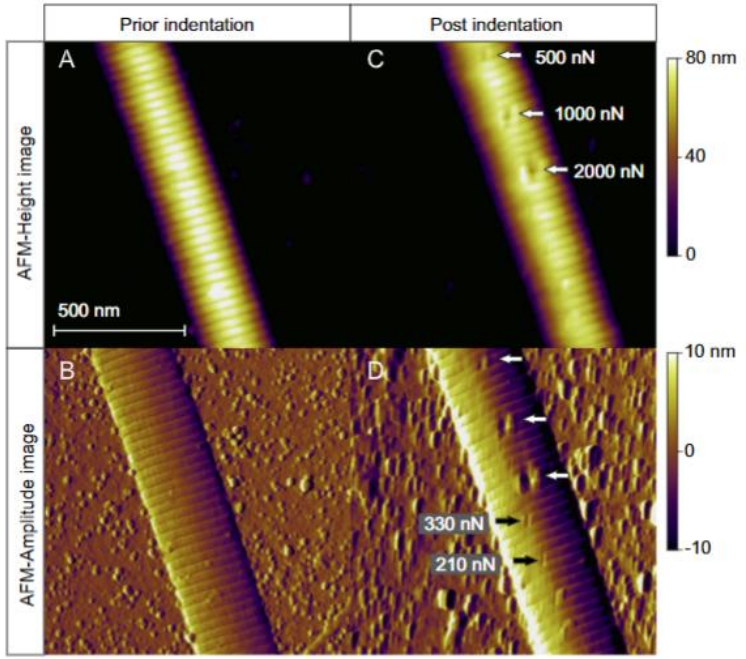

Andriotis et al., 2014, *JMBBM*, 39

Micro-computed tomography

- μCT is a 3D imaging technique utilizing X-rays to see inside an object, slice by slice.

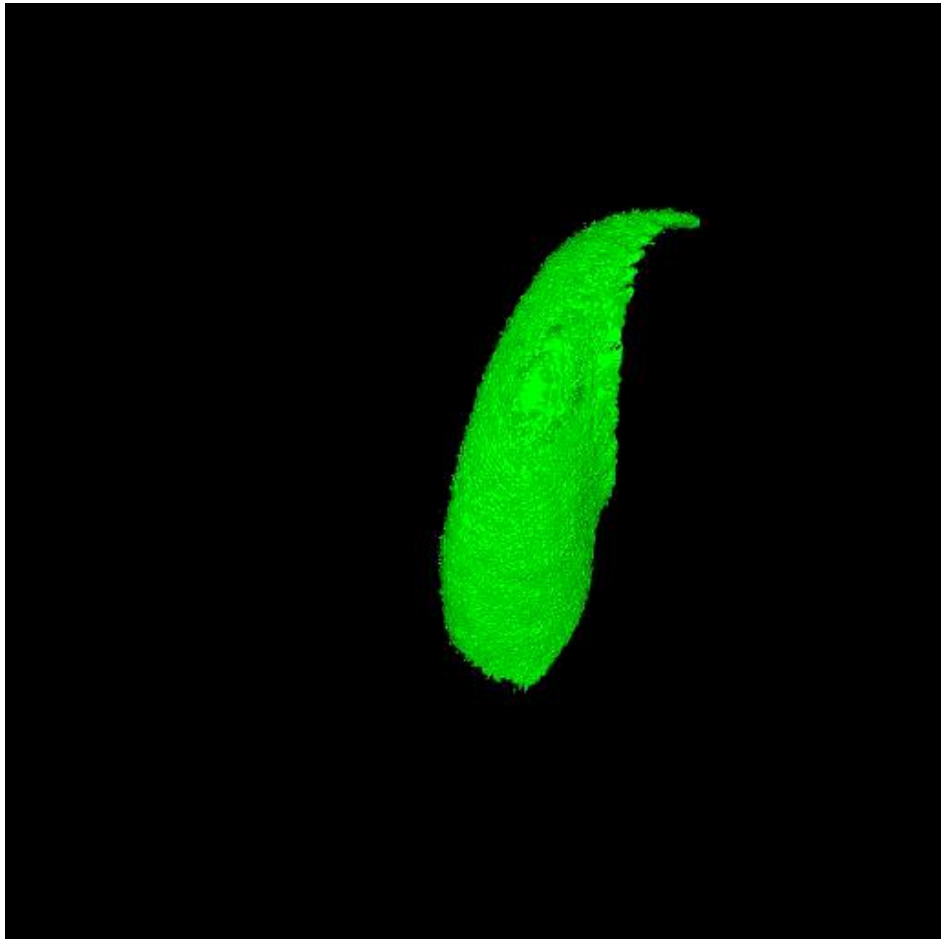

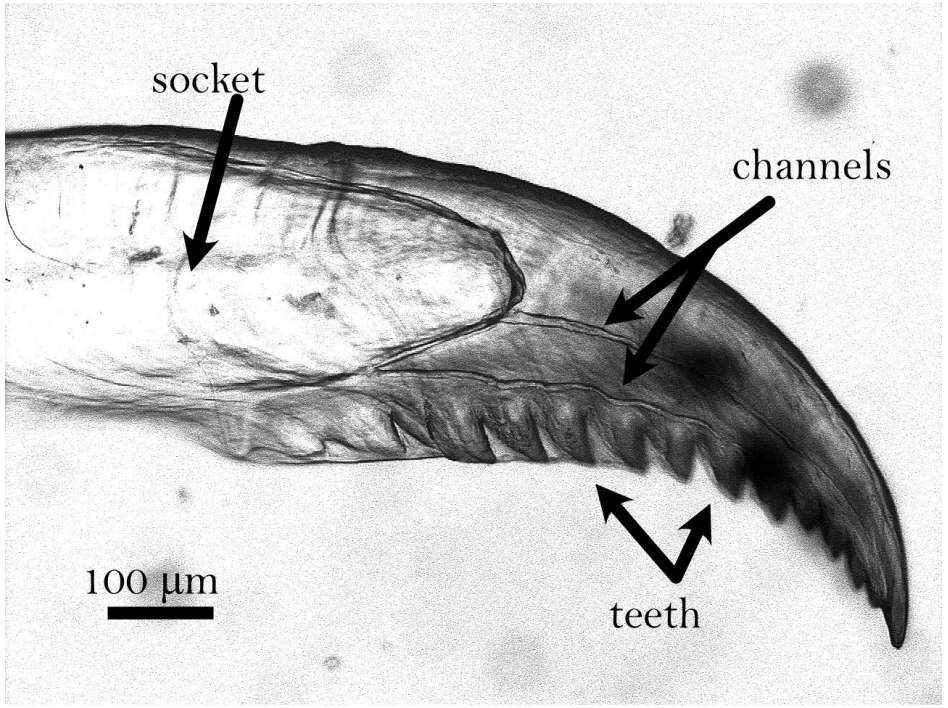

Zelaya-Lainez et al., (2021) Jaws of Platynereis dumerilii: Miniature Biogenic Structures with Hardness Properties Similar to Those of Crystalline Metals, *JOM*